ANL-85-53

ANL-85-53

THREE-DIMENSIONAL THERMAL MODELING OF ELECTRIC VEHICLE BATTERIES

by

Johnsee Lee, K. W. Choi, N. P. Yao,
and C. C. Christianson

ARGONNE NATIONAL LABORATORY, ARGONNE, ILLINOIS

Operated by THE UNIVERSITY OF CHICAGO
for the U. S. DEPARTMENT OF ENERGY
under Contract W-31-109-Eng-38

Argonne National Laboratory, with facilities in the states of Illinois and Idaho, is owned by the United States government, and operated by The University of Chicago under the provisions of a contract with the Department of Energy.

Printed in the United States of America
Available from
National Technical Information Service
U. S. Department of Commerce
5285 Port Royal Road
Springfield, VA 22161

NTIS price codes
Printed copy: A04
Microfiche copy: A01

Distribution Category:
Energy Storage—Electrochemical--
Near-Term Batteries (UC-94ca)

ANL-85-53

ARGONNE NATIONAL LABORATORY
9700 South Cass Avenue
Argonne, Illinois 60439

THREE-DIMENSIONAL THERMAL MODELING OF ELECTRIC VEHICLE BATTERIES

by

Johnsee Lee, K. W. Choi, N. P. Yao,
and C. C. Christianson

Chemical Technology Division

October 1985

TABLE OF CONTENTS

LIST OF FIGURES

LIST OF TABLES

THREE-DIMENSIONAL THERMAL MODELING OF ELECTRIC VEHICLE BATTERIES

by

Johnsee Lee, K. W. Choi, N. P. Yao, and C. C. Christianson

ABSTRACT

A generic three-dimensional thermal model was developed for analyzing the thermal behavior of electric-vehicle batteries. The model calculates temperature distribution and excursion of a battery during discharge, charge, and open circuit. The model takes into account the effects of heat generation, internal conduction and convection, and external heat dissipation on the temperature distribution in a battery. The three-dimensional feature of the model permits incorporation of various asymmetric boundary conditions; thus the effects of cell orientation and packaging on thermal behavior can be analyzed for a multiple-cell battery pack. Various modes of boundary heat transfer such as radiation, insulation, and natural and forced convections were also included in the model.

Model predictions agreed well with the temperature distributions measured in nickel/iron batteries. Application of the thermal model to a closely packed 330-Ah module of five cells indicated that excessive temperature rise will occur upon discharge. Forced air convection is not effective for cooling the module.

To facilitate the use of the model by electric-vehicle designers and battery developers, the computer code for the model was simplified so that calculations can be made on a minicomputer. The flow diagram for the computer code and the input/output specifications are described. A sample calculation is also given to illustrate the procedures involved in using the model for battery thermal analysis.

I. INTRODUCTION

The temperature of batteries and electrochemical cells, owing to the resistive heating and the entropy changes of the reactions, often varies during the operation. In many instances, such temperature variations affect the performance and life of the electrochemical cells and batteries.[1-5] Therefore, it is desirable to control their temperature within a suitable range. In addition, the temperature distribution in cells and multicell modules should be kept uniform to avoid localized degradation and to maintain a balanced utilization of active material. These two requirements, namely, the proper temperature range and uniformity, are particularly important for operating high-energy-density batteries and fuel cells because of their high rate of heat generation.

To achieve proper temperature control of batteries, one needs to understand how the cell design and operating variables affect the thermal behavior. An efficient way of assessing these effects and formulating a thermal controlling scheme is to model mathematically the thermal behavior of a battery under various design and operating conditions. Figure 1 shows the desirable inputs to such a model for electrochemical cells and batteries. Once the cell design specification, the thermal properties, and the electrical performance characteristics of a battery system are given, its temperature distribution and variation can be predicted by the model for different operating and ambient conditions.

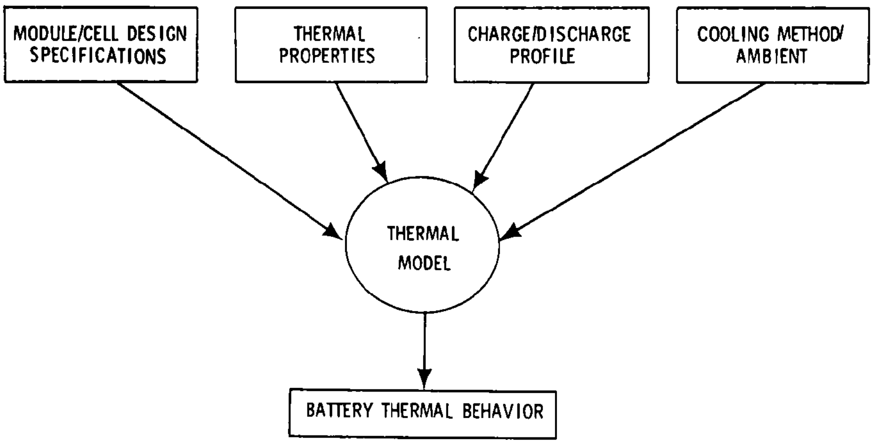

Fig. 1. Inputs to Battery Thermal Model

The first of this type of model was published in 1965 by Gidaspow and Baker.[6] In 1971, Gidaspow et al. gave an extensive analysis on steady-state temperature distribution in fuel cells and batteries.[7] The usefulness of Green's function method in formulating a series solution for the thermal model was demonstrated. In 1978, Choi and Yao[8,9] analyzed the transient two-dimensional temperature distributions for lead-acid batteries by using the finite-difference technique. Their method allows more flexibility in treating complicated boundary conditions. Chen and Gibbard[10,11] adopted a similar method to model the heat transfer in cylindrical and parallelepiped batteries under convective boundary conditions. A review on heat transfer modeling and thermal management of batteries was given by Yao in 1981.[12]

Recently, attention has been focused on modeling full-scale electric vehicle (EV) batteries.[13] A large number of cells or modules are often needed to power an electric vehicle. As a result of the close packing needed for the cells or modules, the dissipation of heat is less efficient. Generally, the temperature rise will be higher, and the temperature gradients will be larger for a collection of cells in comparison with a single cell. The thermal behavior of individual cells and modules in the battery pack is also affected by the asymmetrical boundary conditions imposed by the packaging requirements of the vehicle. A three-dimensional model capable of depicting the thermal interactions among cells and modules is derived in the following discussion. This model allows one to accurately predict the thermal behavior of a full-scale EV battery. This information can then be used to control the battery temperature. The same methodology can be applied to electrochemical cells other than EV batteries.

II. MODEL FORMULATION

The thermal behavior of a full-size battery can be described by integrating thermal models derived for individual cells or modules under appropriate boundary conditions. Therefore, a three-dimensional model for a single cell serves as the building block for analyzing the thermal behavior of a multicell system.

A typical composite cell is schematically represented by Fig. 2. The cell is divided into two regions: the core region and the boundary region. The core, consisting of the stack of electrodes and separators, is the region where electrochemical reactions occur. The temperature distribution in this region is our primary interest. The boundary region, consisting of the cell case and electrolyte surrounding the core, occupies only a small portion of the cell volume. This region provides the contact between the core and the environment outside the cell. In the following, we first formulate an equation that describes the thermal phenomena in the core region. Then, the heat transfer and the heat accumulation in the boundary region are treated in conjunction with the cooling conditions at the external surfaces. This provides boundary conditions for determining the temperature distribution in the core region of the composite cell.

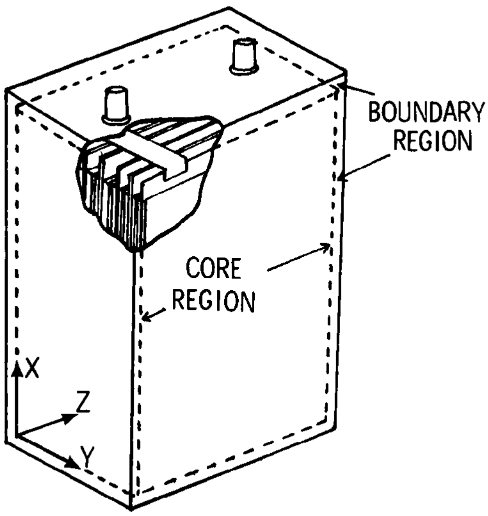

Fig. 2.

Schematic Representation of Three-Dimensional Thermal Model for Typical Composite Cell

A. Core Region

Previous study[14] had shown that because of the intimate contact among electrodes, electrolyte, and separator, the instantaneous temperature difference between components in proximity is often very small ($\sim 10^{-4}$°C). This allows one to consider the composite electrode stack as a quasi-homogeneous medium and to assume that the thermal behavior of the core region can be sufficiently represented by averaged properties such as average specific heat and effective thermal conductivities. One can also assume that the heat generated from various sources can be averaged over any differential volume in the core region. With these approximations, one can write the energy conservation equation, the equation describing the temperature distribution in the core region, as

$$\hat{\rho}C \frac{\partial T}{\partial t} = k_x \frac{\partial^2 T}{\partial x^2} + k_y \frac{\partial^2 T}{\partial y^2} + k_z \frac{\partial^2 T}{\partial z^2} - \hat{\rho}CU_x \frac{\partial T}{\partial x} + \dot{\underline{q}} \tag{1}$$

where $\hat{\rho}$, C, and k are average density, average specific heat, and effective thermal conductivities, respectively; U_x denotes the equivalent convective velocity in the x-direction; and $\dot{\underline{q}}$ is the heat generation rate per unit volume.

The convective velocity, U, here assumed exists only in the x-direction and represents the average motion of a composite mass, which is equivalent to the actual movement of the electrolyte. In most cases, such a movement is caused by the change of electrode porosity as electrochemical reactions occur. The relationship between the porosity change of electrodes and the equivalent convective velocity can be approximated by

$$U_x = -\frac{L_x}{4W_e}\left[W_N \frac{d\epsilon_N}{dt} + W_p \frac{d\epsilon_p}{dt}\right] \tag{2}$$

where L_x is the height of the core region, W_N and W_p are thicknesses of the negative and positive electrodes, ϵ_N and ϵ_p are porosities of the negative and positive electrodes, W_e is the total thickness of the positive and negative electrode. The rate of porosity change can be further approximated by the differences in molar volume ($\tilde{V}$) between the reactants and products of the ongoing reaction

$$\frac{d\epsilon}{dt} = \frac{i}{nFW_e}\left[\sum_{\text{product}} s_j \tilde{V}_j - \sum_{\text{reactant}} s_j \tilde{V}_j\right] \tag{3}$$

where i is the superficial current density, j represents different species of products and reactants, s is the stoichiometric constant for the reaction, n is the number of electrons transferred, and F is Faraday's constant.

The $\dot{\underline{q}}$ in Eq. 1 is the local rate of heat generation per unit volume in the core region. A detailed analysis of thermodynamic changes associated with electrochemical reactions was presented by Gibbard.[15] Recently, Bernardi et al. derived a general equation for estimating heat generation rates in battery systems.[16] For simplicity, $\dot{\underline{q}}$ may be written as

$$\dot{\underline{q}} = \frac{i}{W_e}\left[V + \frac{\Delta H^\circ}{nF} + \frac{\Delta C_p}{nF}(T - T_{ref})\right] \tag{4}$$

where i is the local current density; W_e is the thickness of a composite element; V is the cell voltage, which varies with time during cell operation; $\Delta H°$ is the heat of the discharge reaction at reference temperature T_{ref}; ΔC_p is the change in the sum of the partial molar heat capacities of species involved in the cell reaction. Here the sign conventions for the charge (or electrolysis) and discharge are defined as follows: $\Delta H° < 0$ for exothermic and $\Delta H° > 0$ for endothermic reaction; $i > 0$ for charge and $i < 0$ for discharge; and V always remains positive.

If more than one reaction occurs, Eq. 4 is written as

$$\underline{\dot{q}} = \frac{i}{W_e}\left[V + \sum_j \zeta_j \frac{\Delta H_j^\circ}{n_j F} + (T - T_{ref}) \sum_j \zeta_j \frac{\Delta C_{p_j}}{n_j F}\right] \tag{5}$$

where V is the voltage, and ζ_j is the fraction of total current contributed by reaction j. In general, current distribution at the electrode is not completely uniform. Therefore, i may vary with location at the electrode. Besides, i may vary with time depending on how the cell is operated, i.e., whether the total current or cell voltage is controlled. In the present analysis, it is assumed that the function $i = i(t, x, y, z)$ is predetermined. Similarly, the variation of cell voltage with time, $V = V(t)$, is also assumed to be a given function.

With both i and V prescribed, the heat generation rate ($\underline{\dot{q}}$) in Eq. 5 can be determined. However, the requirement of knowing i and V *a priori* imposes a limitation on the predictive power of the model. The heat generation rate cannot be calculated without knowledge of the variations of i and V during cell operation. Theoretically i, V, and T are dependent upon one another. Therefore, determining i and V without knowing T is difficult. In practice, however, there are cases when i and V are not significantly affected by T. For example, the voltage-time curve of aqueous secondary batteries during discharge does not change significantly with temperature; thus, it can be used to calculate the rate of heat generation.

B. Boundary Region

The boundary region, as shown in Fig. 2, designates the cell case plus the electrolyte surrounding the core region. Since electrochemical reactions occur only at the electrodes, no heat generation occurs in the boundary region. In terms of heat transfer, the boundary region separates the core region from the outside environment and thus imposes an additional barrier to heat dissipation. However, the electrolyte in this region absorbs heat generated in the core region and thus serves as a heat sink. To account for the effect of the boundary region and to provide a direct relation between the core region and the external environment, the following equation can be used for all three directions (n = x, y, or z):

$$-k_n \left.\frac{\partial T(n)}{\partial n}\right|_{n=0,L} = h(T_s - T_\infty) + e\delta(T_s^4 - T_\infty^4) + \rho_B C_{p,B} H_B \frac{\partial T_B}{\partial t} - \rho_\ell C_\ell T U_x \tag{6}$$

where T is the temperature at the surface of the core region; T_s is the temperature at the external cell surface; T_B is the average temperature of the boundary region, taken here to be the arithmetic average of T and T_s; e is the emissivity of the cell surface; δ is the Stefan-Boltzmann constant; H_B, ρ_B and $C_{p,B}$ are the thickness, density, and specific heat of the boundary region; h is the heat transfer coefficient at the external surfaces of the cell; ρ_ℓ and C_ℓ are density and specific heat of liquid electrolyte; and L is the total length of the core region in each direction. The left-hand side of Eq. 6 represents the heat flux at the interface between the core and the boundary region due to conduction outward from the core region. The first term of the right-hand side is the heat dissipation by convective heat transfer at the outside surface; the second term is the heat dissipation by radiative heat loss; and the third term accounts for the heat absorbed by the boundary region. In addition, the mass in the boundary region may vary with time. For example, as a result of the upward movement of electrolyte in the core region, the amount of heat flux carried by the electrolyte into the boundary needs to be accounted for. Therefore, a convective term "$-\rho_\ell C_\ell TU_x$" was needed for the right-hand side of Eq. 6; C_B and H_B vary with time.

To establish a relationship between T and T_s, one assumes that the temperature drop through the boundary region is due to an overall heat-transfer resistance imposed by the electrolyte and cell case. If, for this relationship, the convective flow in the boundary region is negligible and the radiative effect is small, the following equation can be derived, based on the same principle used in determining heat conduction through a composite material:

$$T_s = C_B T + (1 - C_B) T_\infty \tag{7}$$

where $$C_B = \left(1 + \frac{h\, H_\ell}{k_\ell} + \frac{h\, H_c}{k_c}\right)^{-1} \tag{8}$$

where H_ℓ and k_ℓ are the thickness and thermal conductivity of liquid electrolyte, and H_c and k_c are the same for the cell case material. Substituting Eq. 7 into Eq. 6 and linearizing the radiative term, one obtains

$$-k_n \left.\frac{\partial T(n)}{\partial n}\right|_{n = 0,\, L} = h\, C_B(T - T_\infty) + e\delta \left[(4\, C_B - 3)T^4 - T_\infty^4 + 4\, T^3\, T_\infty\, (1 - C_B)\right] + (1 + C_B)\, \frac{\rho_B\, C_{p,B}\, H_B}{2} \frac{\partial T}{\partial t} - \rho_\ell C_\ell T U_x \tag{9}$$

This is the boundary condition for Eq. 1, the equation defining the temperature distribution in the core region. One needs to use different coefficients for boundaries in different spatial directions when the heat transfer coefficient (h) and the amount of electrolyte in the boundary region are not identical in each direction.

Besides the boundary conditions, an initial condition is required to completely define the temperature distribution of a cell. The initial condition is

$$T\ (x,\ y,\ z,\ t) = T_o\ (x,\ y,\ z,\ t) \quad \text{at } t = 0 \tag{10}$$

III. DIMENSIONLESS ANALYSIS AND APPLICATIONS TO NICKEL/IRON BATTERY

To obtain generalized characteristics of thermal behavior for electrochemical cells and batteries and to reduce the number of parameters, the model parameters were normalized as follows:

$$T^* = T(n)/T_o \tag{11}$$

$$t^* = t/t_L \tag{12}$$

$$x^* = x/L_x \tag{13}$$

$$y^* = y/L_y \tag{14}$$

$$z^* = z/L_z \tag{15}$$

$$V^* = V/V_{avg} \tag{16}$$

where T_o is the initial temperature of the cell; t_L is the time elapsed during charge or discharge; L_x, L_y, and L_z are the height, width, and thickness of the core region; V_{avg} is the average cell voltage during the operation. By reformulating Eqs. 1, 5, 9, and 10 using the newly defined variables, one can obtain the following four types of dimensionless parameters:

Internal Heat Transfer (i = x, y, or z)

$$k_i^* = k_i \; t_L/L_i^2 \; \rho \; C_p \tag{17}$$

$$U_i^* = U_i \; t_L/L_i \tag{18}$$

Boundary Heat Transfer

$$h_i^* = h_i \; L_i/k_i \tag{19}$$

$$E_i^* = e_i \; \delta \; T_o^3 \; L_i/k_i \tag{20}$$

$$B_i^* = \rho_B \; C_{p,B} \; H_B \; L_i/k_i \; t_L \tag{21}$$

$$C_B = (1 + h \; H_\ell/k_\ell + h \; H_c/k_c)^{-1} \tag{22}$$

Heat Generation

$$G^* = I \; V_{avg} \; t_L/\rho \; C_p \; L_x \; L_y \; L_z \; T_o \tag{23}$$

$$H^* = \Delta H^\circ/nF \; V_{avg} \tag{24}$$

$$\Delta C_p^* = \Delta C_p\ T_o/nF\ V_{avg} \tag{25}$$

Ambient Condition

$$T_\infty^* = T_\infty/T_o \tag{26}$$

The thermal characteristics of a particular battery or electrochemical system can often be represented by the numerical values of these dimensionless parameters. For example, k^* and U^* represent the magnitude of normalized thermal conductivity and convective velocity in the core region. In the boundary region, the B^* represents the thermal capacitance of the cell case and the electrolyte surrounding the electrode stack; the C_B, ranging from 0 to 1, is a correction factor accounting for the thermal resistances imposed by the boundary region. At the external surfaces of the cell, the rate of heat dissipation by convection and radiation can be represented by h^* and E^*, respectively. In the core region where electrochemical reactions occur, the heat generation rate is proportional to the sum of G^* (the ratio of specific energy to initial specific heat content) and H^* (the normalized standard heat of reaction), adjusted by ΔC_p (the normalized enthalpy change with temperature). A final independent parameter is T_∞^*, the ratio of ambient temperature to the initial cell temperature. The typical values of these dimensionless parameters for a nickel/iron cell fabricated by Eagle-Picher Industries, Inc.,[17] are given in Table 1.

Table 1. Typical Numerical Values of Dimensionless Thermal Parameters for a Nickel/Iron Cell during Discharge

Thermal Parameters	Typical Values
G^*	$-0.6 \sim -0.9$
H^*	$0.3 \sim 2.0$
k^*	$0.4 \sim 1.2$
U^*	0.001
B^*	0.2
C_B	0.8
h^*	$0.3 \sim 1.5$
E^*	0.02
T_∞^*	1.0

With the definitions of these dimensionless variables and parameters, Eqs. 1, 5, 9, and 10 can be rewritten in dimensionless form:

$$\frac{\partial T^*}{\partial t^*} = k_x^* \frac{\partial^2 T^*}{\partial x^{*2}} + k_y^* \frac{\partial^2 T^*}{\partial y^{*2}} + k_z^* \frac{\partial^2 T^*}{\partial z^{*2}} - U_x^* \frac{\partial T^*}{\partial x^*}$$

$$+ G^* \left[V^* + H^* + \Delta C_p^* \left(T^* - T_{ref}^* \right) \right] \tag{27}$$

The boundary condition is

$$- \frac{\partial T^*}{\partial n^*} \bigg|_{n^* = 0,1} = C_B h_n^* \left(T^* - T_\infty^* \right) + E_n^* \left(T^{*4} - T_\infty^{*4} \right) +$$

$$4 \left(C_B - 1 \right) E_n^* T^{*3} \left(T^* - T_\infty^* \right) + \left(1 + C_B \right) \frac{B_n^*}{2} \frac{\partial T^*}{\partial t^*} - U_x^* T^* \tag{28}$$

The initial condition is

$$T^* = 1 \longrightarrow \text{at } t^* = 0 \tag{29}$$

Equations 27-29 determine the generic patterns of temperature distribution and excursion for batteries. The set of equations can be solved by the finite difference method to obtain an understanding of the effects of dimensionless parameters on battery thermal behavior. Based on the parameter values given in Table 1, the system of equations was solved by the implicit alternating-direction scheme.[18] The results of the dimensionless calculations are qualitatively summarized in Table 2. The numerical solution was found stable over a wide range of parameter values.

In Table 2, those parameters having significant effects on the total cell temperature rise and temperature uniformity within the cell during discharge are marked by "X." In terms of temperature uniformity in the battery, h^* and C_B have the strongest effect. As the cell size becomes larger or the discharge rate becomes higher, the effects of k^* and U^* become more significant.

In terms of the effect on cell temperature rise, more parameters are involved. By far the most important parameters in determining temperature rise are G^* and H^*. Both parameters are directly related to the properties of electrochemical reactions occurring inside the battery. The ambient condition, T_∞^*, and external heat removal parameter, h^*, also have significant influence on the magnitude of temperature rise. At high rates (C or C/2, i.e., one-hour or two-hour rate) of discharge, the thermal resistance and capacitance imposed by the cell case and the surrounding electrolyte, represented by C_B and B^*, become important. However, their effects diminish as the size of the cell increases. This is mainly due to the reduction of external surface area per unit volume. In addition, the internal conduction parameter, k^*, becomes more important in larger cells. In most cases, the effects of radiation on total heat loss are small ($\sim$10% of convection), except at low discharge rates

Table 2. The Relative Importance of Thermal Parameters

Thermal Parameters	Total Cell Temp. Rise: High Rate Discharge[a]	Total Cell Temp. Rise: Low Rate Discharge[b]	Cell Temperature Uniformity
G^*	X	X	
H^*	X	X	
k^*	X		X
U^*			X
B^*	X		
C_B	X		X
h^*	X	X	X
E^*		X	
T^*_∞	X	X	

[a]C or C/2.
[b]C/3 or less.

(C/3 or less) under natural convection where the effects of internal conduction, convection, and boundary resistances become secondary, and the radiative heat loss has the same magnitude of effect as external convection.

Another factor affecting the thermal behavior of a battery is the dimensionless cell voltage, $V^*(t)$, which was treated here as a given function. A standard constant-current discharge curve was used throughout this analysis. If different types of $V^*(t)$ (e.g., pulsed discharge) are used, both temperature rise and temperature uniformity of the battery will not be the same as those from constant-current discharge.

Because of the interdependency and the large number of parameters involved, the quantitative effects of isolated dimensionless parameters often have little practical use. Therefore, only the qualitative effects of the dimensionless analysis have been discussed up to this point. In the following, the model is applied to actual batteries and cells, and the results are presented in specific dimensions rather than in dimensionless form.

IV. RESULTS AND DISCUSSION

A typical result of model application is shown in Fig. 3, in which the temperature distribution is presented for the mid-height cross section of a three-module EV-3000 lead-acid battery fabricated by Globe Battery Division, Johnson Controls, Inc.[19] The result shows that the average temperature of the battery increased from 25°C to approximately 33°C after two hours of charging at a 3-h rate. The flat temperature profile at the center of each module indicates that the internal thermal resistance is relatively small compared with that at the boundary. While the small air gap between modules provides a heat sink, it is not effective in dissipating heat under the natural convection condition. The result also shows that a higher temperature exists near the surface area where modules face one another.

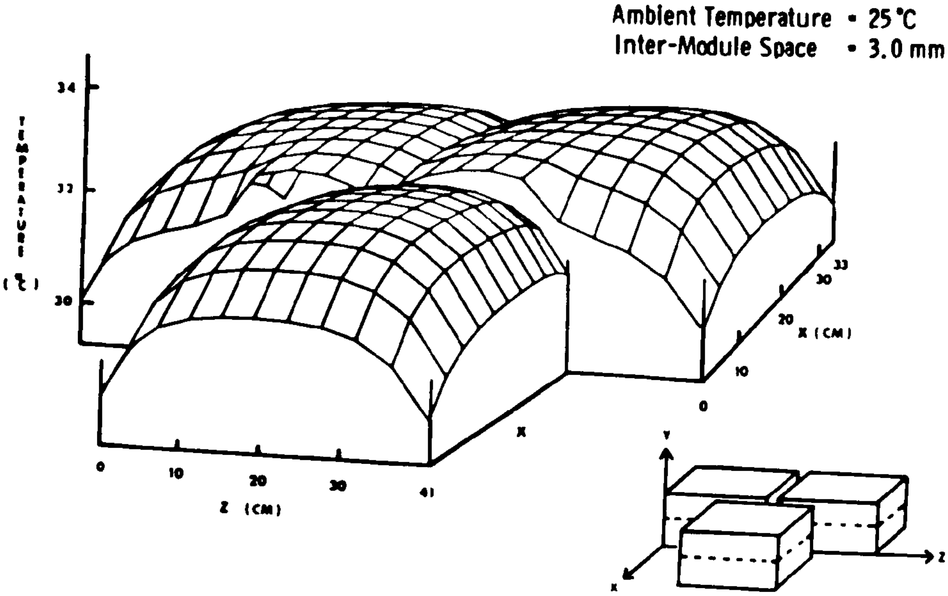

Fig. 3. Calculated Temperature Distribution at Mid-Height Cross Section of Three-Module Lead-Acid Battery after Two Hours of Charge at 3-h Rate under Natural Convection Cooling

The model has also been applied to study the thermal behavior of nickel/iron batteries[20] and to compare model calculations with experimentally measured temperature distributions. The details of the experimental set-up and procedures were described elsewhere.[21] The temperature variations were measured by 15 thermocouples embedded inside a 150-Ah nickel/iron cell (fabricated by Eagle-Picher). The cell was charged and discharged within a specially instrumented test fixture that provides a well-defined boundary condition around the test cell. The cell voltages recorded during the discharges were fitted to Shepherd's equation so that the instantaneous voltage variations needed for modeling heat generation can be easily calculated. Figures 4 and 5 show the measured data and the temperature profiles predicted by the model in

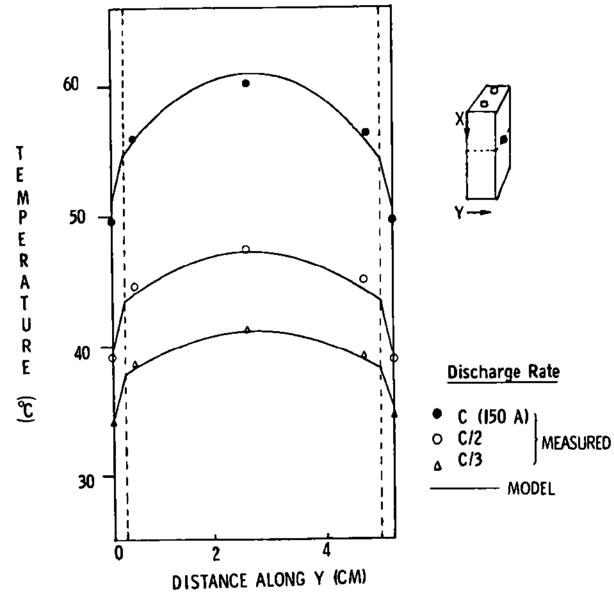

Fig. 4.

Measured and Calculated Temperature Profiles in Y-direction at the Center of 150-Ah Nickel/Iron Cell after Full Discharges at Three Different Rates under Moderate Forced Convection Cooling

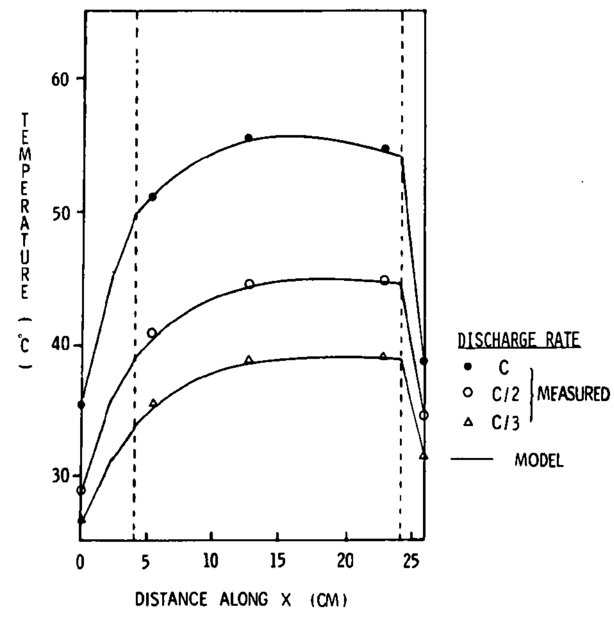

Fig. 5.

Measured and Calculated Temperature Profiles in X-direction at the Center of 150-Ah Nickel/Iron Cell after Full Discharges at Three Different Rates under Moderate Forced Convection Cooling

two different spatial directions, x and y. In both figures, the dashed lines indicate the point of separation between the core and boundary regions. The cell dimensions and physical properties used in these calculations are listed in Table 3. The numerical values of the effective heat capacity and the thermal conductivities of the cell were estimated from separate experimental data.[21]

In both the x- and y-directions for three different rates of discharge, the model predictions agree well with the experimental measurements. The temperature distributions in the z-direction are similar to those of the

Table 3. Physical Parameters Used to Model Temperature Variations of 150-Ah Ni/Fe Cell during Discharge

$\rho \hat{C}_p$	2.91	$J/cm^3 \cdot K$	e	0.8
k_x	12.4	$W/(m \cdot K)$	h	2-5 m/s
k_y	1.47	$W/(m \cdot K)$	ξ	1.0
k_z	8.5	$W/(m \cdot K)$	L_x	4.9 cm
U_x	0.5×10^{-6}	m/s	L_y	24.5 cm
ΔH°	-286330	J/mol	L_z	18.3 cm
ΔC_p	30	J/mol		

y-direction and thus are not shown here. The results in Figs. 4 and 5 also show that a significant thermal resistance exists in the boundary region, as indicated by the sharp temperature drop between the core region and the external surfaces of the cell. Such temperature drops are mainly caused by the relatively nonconductive cell case material.

In Fig. 6, the temperature distributions (in y-direction) of cells having different case materials are compared. The large temperature drops through boundary regions disappear when the cell case material is changed from plastic ($\kappa = 0.173$) to metal ($\kappa = 78.0$). The reduction of thermal resistance also helps reduce the average temperature of the cell. The thermal resistance caused by the cell case plays a more important role as the cell temperature becomes higher. At the end of discharge, about 30% of total temperature drop between the cell and the ambient air is due to the boundary resistance. In this particular case, the major heat transfer barrier (about 50%) lies in the air stream outside the cell.

The cell temperature rises measured by the thermocouple located near the center of the external cell surface are compared with the model predictions in Fig. 7 for three different discharge rates. Again, the agreement between the model calculations and experimental results is quite good. Using the same conditions, the results of model calculation for continuous discharge, open circuit, and charge are shown in Fig. 8. The temperature differences between the center and corner of a cell are as large as 10°C. The time required to cool down the cell can also be estimated from the calculation.

The effects of air cooling rate and ambient temperature on the maximum temperature rise of a battery can also be calculated by the model. These effects are shown in Fig. 9 for a 330-Ah nickel/iron cell. The temperature rise (ΔT) and ambient temperature (T_∞) in the figure are normalized by

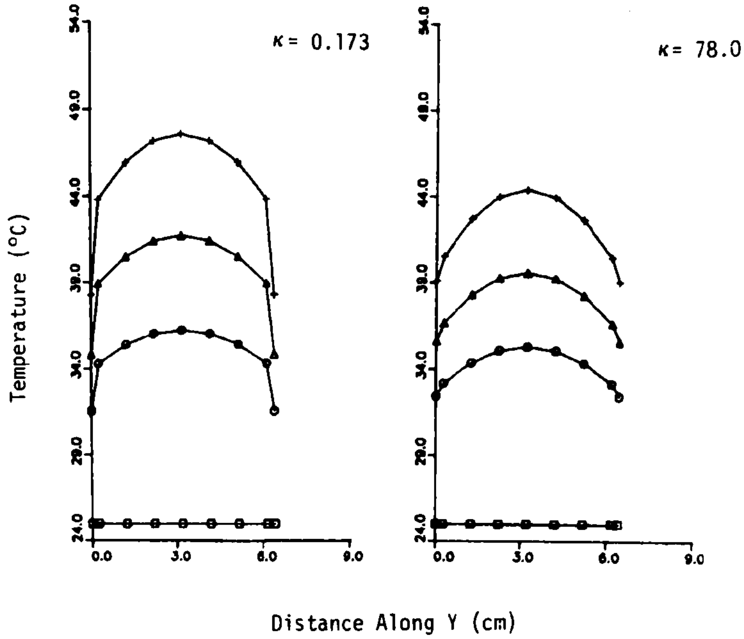

Fig. 6. Temperature Profiles of Cells Having Different Thermal Conductivities of Cell Case Material. (Curves represent temperature profiles in Y-direction at the center of the cell and at different depths of discharge.)

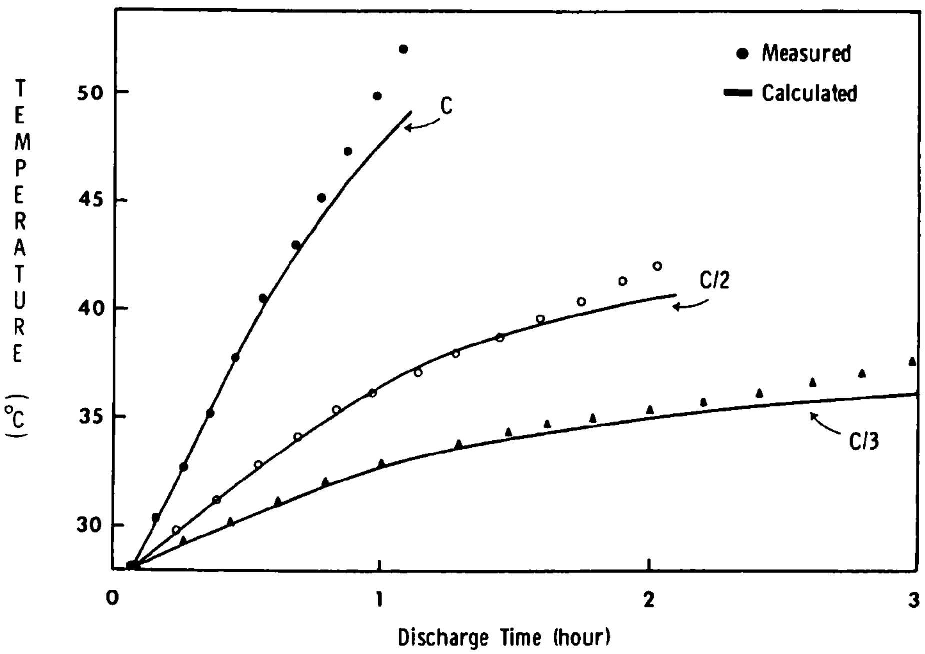

Fig. 7. Measured and Calculated Temperature Rises of Nickel/Iron Cell during Three Constant-Current Discharges under Moderate Forced Convection Cooling

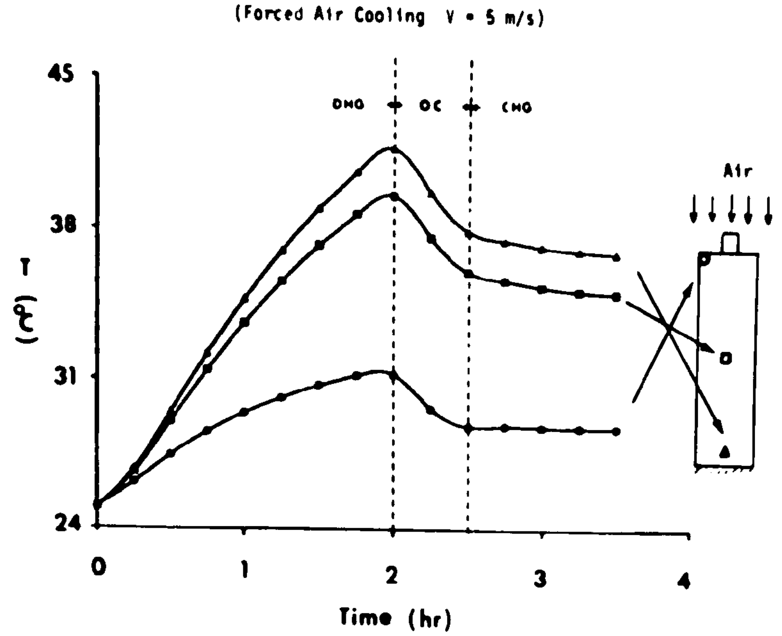

Fig. 8. Calculated Temperature Excursion of a Nickel/Iron Cell during Discharge (DHG), Open Circuit (OC), and Charge (CHG) under Moderate Forced Convection Cooling

dividing by the initial cell temperature (T_o); as a consequence, the relationships hold for various initial temperature conditions. In Fig. 9, the corresponding ambient temperatures and the predicted temperature rises at an initial temperature of 25°C (298 K) are given in parentheses. The cell temperature rise decreases as the cooling rate increases. However, the effectiveness of air cooling diminishes as the normalized cooling rate, h^* as defined in Eq. 19, exceeds 1.0, which corresponds to an air velocity of about 20 m/s for a 330-Ah cell.

When several cells are packed into a module, the degree of temperature variation during charge/discharge becomes quite different from that for a single cell. There are several design parameters affecting the thermal behavior of a module: ampere-hour capacity, number of cells per module, packing and cooling orientations, and space between cells. Examination of the effects of these parameters on the thermal behavior of a nickel/iron battery was reported elsewhere.[20] Using a 6-V, 330-Ah nickel/iron module consisting of five closely packed cells fabricated by Eagle-Picher as an example, the maximum temperature rise after three hours of constant-current discharge was determined to be significantly higher than that for a single cell. A cross-sectional temperature distribution in such a module at a cooling air velocity of 5 m/s is shown in Fig. 10. The temperature of the two side cells is reduced while all three center cells remain unaffected. The maximum temperature of the module after the discharge exceeds the 55°C temperature limit set by the battery manufacturer. Thus, the forced air cooling is not an

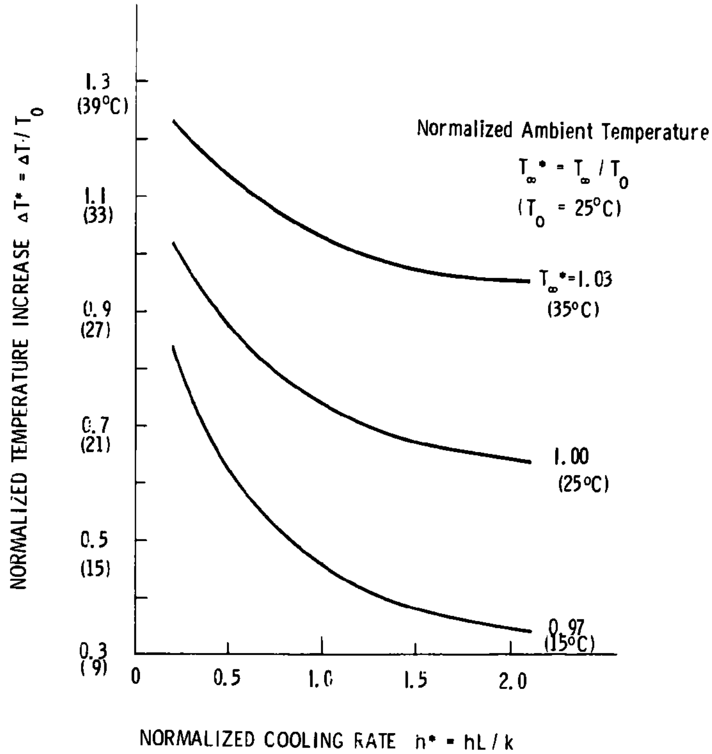

Fig. 9. Effects of Air Cooling Rate and Ambient Temperature on the Maximum Temperature Rise of a 330-Ah Nickel/Iron Cell after 3-h Constant Discharge

effective means for lowering the center temperature of a closely packed 330-Ah nickel/iron module. An air space between individual cells or other means of cooling may be needed to control the temperature of the module. Similarly, the model can be used to aid the design of a thermal management system for a full-scale EV battery pack, which may consist of more than one hundred cells.[20]

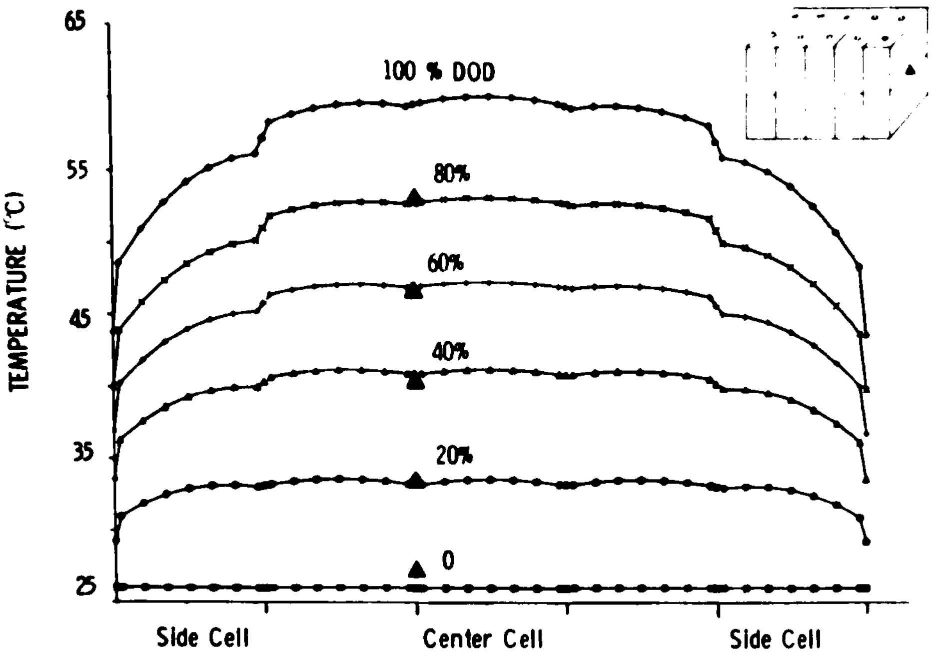

Fig. 10. Temperature Profile in Y-direction at the Center of Closely Packed 330-Ah Nickel/Iron Module (five cells) during a 3-h Constant-Current Discharge. (Solid triangles are measured temperatures.)

V. MODEL COMPUTER CODE

To facilitate the use of the thermal model, a flow diagram for the model computer code is shown in Fig. 11. (The complete computer code is available through the Chemical Technology Division, Argonne National Laboratory.)

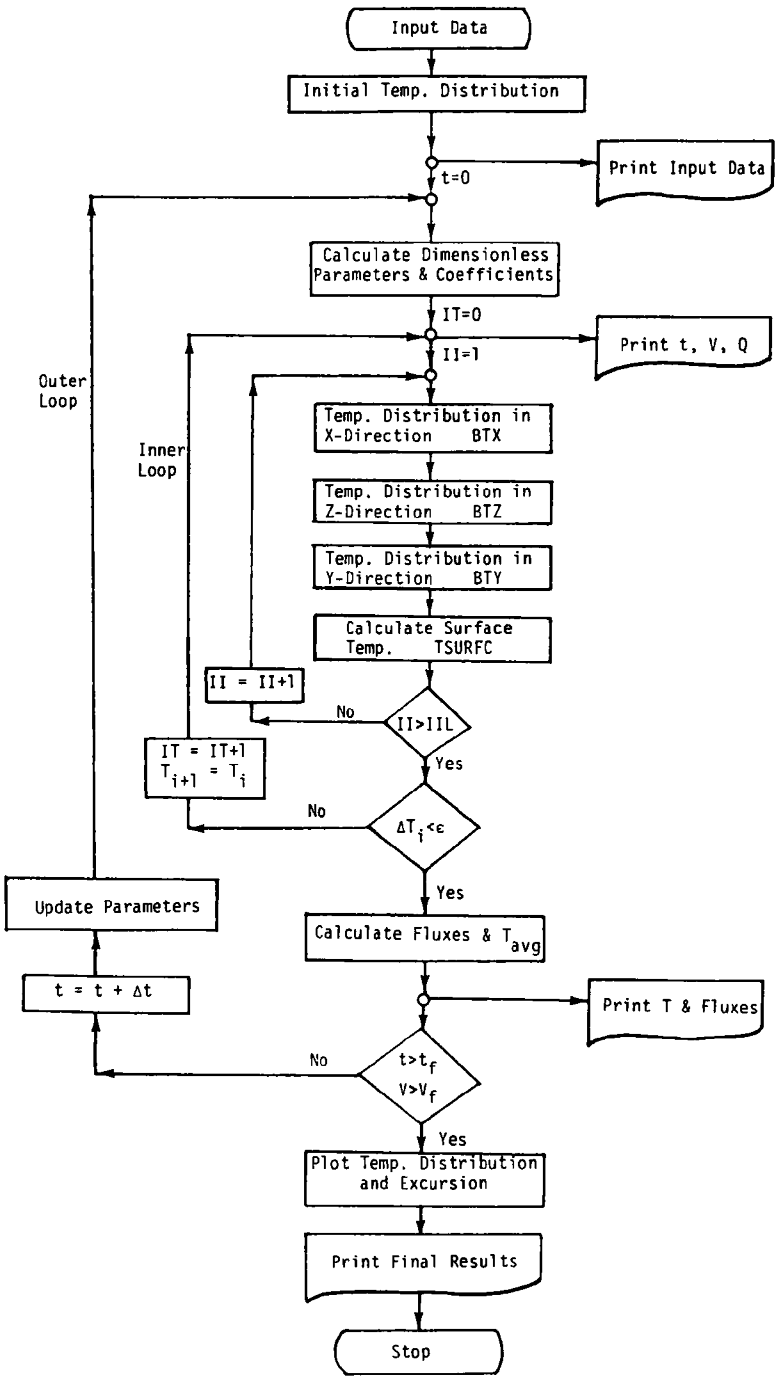

Fig. 11. Flow Diagram for the Thermal Model Computer Code

Input data can be such factors as the cell size, cell/module dimensions and design specifications, the thermal properties of electrolyte, electrode stack, cell case material, the cell voltage curve for the desired discharge profile, ambient temperature, cooling air flow rate, cell/module packaging orientation, and initial cell temperature. The computer model calculates the temperature distribution by the "time-stopping" approach. In other words, the entire discharge process is divided into a number of small time intervals. The model calculates temperature variation over three-dimensional space (x, y, z) for a particular time interval by assuming a quasi-steady state. Once $T = T(x, y, z, t_o)$ is obtained, the calculation proceeds to the next time interval. The dimensionless parameters and heat transfer coefficients are updated at each time-step.

Within each time interval (Δt), the temperature distribution for each module (or cell) is approximated by numerical iteration of the governing equation in the x-, y-, and z-directions. After the iterations in three directions for all modules (or cells) are completed, the resulting temperature distributions are compared with the initially assumed temperature distributions. If the deviations between the newly calculated temperature distribution and the previously assumed value are smaller than a pre-assigned tolerance (e.g., 10^{-4}) at all nodes, then the iteration converges, and the temperature distribution is finalized for that time interval. If the deviation at any node is greater than the tolerance, iteration continues until it converges. After printout of the results for the time-step, calculation proceeds to the next time-step until it reaches the cut-off voltage or assigned termination time.

At the end of the discharge profile, the detailed temperature distributions are printed, and temperature profiles at selected time and locations in the cells are plotted for quick visualization of the results.

There are 15 subroutines and functions attached to the main program of the model. The name and purpose of each subroutine are as follows:

1. BTX
2. BTY
3. BTZ

} to perform temperature iterations in x-, y-, and z-directions, respectively

4. ELOG - to provide iterative solver for simultaneous equations

5. TAVG - to calculate average temperature at each of the external surfaces of battery

6. HBOUND - to provide heat transfer coefficients at all boundaries of battery

7. IFAC - to calculate factorial of K

8. F - to provide functional value for solving cut-off time

9. TBOUND - to define surface temperature at all surfaces of batteries

10. TSURFC - to calculate surface temperature based on internal battery temperature distributions

11. SUROND - to define the contact and orientation of cells and the arrangement of modules in a battery pack

12. PLOT - to generate three-dimensional temperature distribution plots

13. TDIS - to store the calculated temperature profiles along each axis at successive times for plotting

14. PLOT2 - to generate the temperature profile along x-, y-, and z-axes and temperature history along discharge time

15. HQEQ - to calculate total flux of heat dissipation by convection and radiation at each surface

There are two external software packages used:

1. ZFALSE - a subroutine from IMSL Inc. (Houston, TX), used to obtain zero of a function by <u>regula falsi</u> method

2. DISSPLA - a plotting software from ISSCO (Integrated Software System Corp., San Diego, CA 92121), used to generate all the plots

Input to the Model

The following is a list of the input data required for the computer model. The definition, unit, and format of each input are also given.

```
C    *****INPUT DATA : *****
C      UNITS: TIME (SECOND)
C             TEMPERATURE (DEGREE C)
C             MODULE/CELL DIMENSIONS (METER)
C
C    CONTROL TIME, DIMENSIONS, AND NO. OF STEPS
C
      READ(5,101) XNSTEP,RXL,RYL,RZL
C     XNSTEP: NO. OF TIME-STEPS TO BE USED IN MODELING
C     RXL   : REAL EXTERNAL LENGTH OF CELL/MODULE IN X DIRECTION
C     RYL   : REAL EXTERNAL LENGTH OF CELL/MODULE IN Y DIRECTION
C     RZL   : REAL EXTERNAL LENGTH OF CELL/MODULE IN Z DIRECTION
C
      READ(5,102) TINI,TIMEDL,TIMECA
C     TINI  : INITIAL BATTERY TEMPERATURE
C     TIMEDL: TIME TO TERMINATE DISCHARGE IF BATTERY OPERATION STARTS
C             WITH DISCHG.;TIME TO INITIATE DISCHG IF STARTS WITH CHARGE
C     TIMECA: TIME TO TERMINATE CHARGE IF OPERATION STARTS WITH CHARGE;
C             TIME TO INITIATE CHARGE IF STARTS WITH DISCHARGE.
C             NOTE--IF TIMEDL<TIMECA, STARTS WITH DISCHARGE. VISE VERSA.
C
      READ(5,102) TO,XNWRT,TIMFL
C     TO    : AMBIENT TEMPERATURE (TEMPERATURE OF SURROUNDING AIR)
C     XNWRT : NO. OF STEPS AT WHICH EXTENSIVE RESULTS WILL BE PRINTED.
C     TIMFL : MAXIMUM LENGTH OF TIME OF BATTERY OPERATION.
C
C    CELL SPECIFICATIONS AND PHYSICAL AND THERMODYNAMIC PROPERTIES
C
      READ(5,102) THEMCX,THEMCY,THEMCZ
C     THEMCX: EFFECTIVE THERMAL CONDUCTIVITY OF CORE REGION
C             IN X DIRECTION (WATTS/M-K)
C     THEMCY: SAME AS ABOVE, IN Y DIRECTION
C     THEMCZ: SAME AS ABOVE, IN Z DIRECTION
C
      READ(5,102) CEC,CED,GCFH
C     CEC   : CURRENT EFFICIENCY OF CHARGE (0--1.)
C     CED   : CURRENT EFFICIENCY OF DISCHARGE (0--1.)
C     GCFH  : COEFFICIENT ACCOUNTS FOR GASSING EFFECT ON THERMAL
C             CONDUCTIVITIES IN CORE REGION
C
      READ(5,101) VVX,VVY,VVZ,DENEL
C     VVX   : EQUAVELENT CONVECTIVE VELOCITY OF ELECTROLYTE (M/SEC)
C             IN X DIRECTION DUE TO CHANGE IN ELECTRODE POROSITY
C     VVY   : SAME AS ABOVE, IN Y DIRECTION
C     VVZ   : SAME AS ABOVE, IN Z DIRECTION
C     DENEL : DENSITY OF ELECTROLYTE (KG/M**3)
C
      READ(5,101) AREAE,DHG,DCR,DCG
C     AREAE : SUPERFICIAL REACTION AREA PER SIDE OF ELECTRODE (M**2)
C     DHG   : STANDARD HEAT OF DISCHARGE REACTION AT REFERENCE T=298K
C             (JOULE/MOLE); DHG<0 FOR EXOTHERMIC REACTION
C     DCR   : AVERAGE SPECIFIC HEAT OF REACTING SPECIES (J/MOLE-K)
C     DCG   : SAME AS ABOVE, FOR GASSING REACTION
C
      READ(5,101) WGTBAT,WGTERM,WGCOVR,VOLEL
C     WGTBAT: WEIGHT OF BATTERY (KG)
C     WGTERM: WEIGHT OF TERMINAL (KG)
C     WGCOVR: WEIGHT OF BATTERY COVER (KG)
C     VOLEL : VOLUME OF ELECTROLYTE (M**3)
C
      READ(5,101) CPEL,CPSOLD,CPWP,THERKL
C     CPEL  : AVERAGE SPECIFIC HEAT OF ELECTROLYTE (J/KG-K)
C     CPSOLD: AVERAGE SPECIFIC HEAT OF SOLID SPECIES IN CORE
C     CPWP  : SPECIFIC HEAT OF PLASTIC CELL CASE
C     THERKL: THERMAL CONDUCTIVITY OF ELECTROLYTE
C
```

```
      READ(5,102) XLAIR,YLAIR,ZLAIR                                      THE01630
C     XLAIR : HEIGHT OF AIR SPACE IN X DIRECTION OF BOUNDARY REGION (M) THE01640
C     YLAIR : SAME AS ABOVE, IN Y DIRECTION                              THE01650
C     ZLAIR : SAME AS ABOVE, IN Z DIRECTION                              THE01660
C                                                                        THE01670
      READ(5,102) BELX1,BELY1,BELZ1                                      THE01680
C     BELX1 : THICKNESS OF ELECTROLYTE IN BOUNDARY REGION AT X1 (M);    THE01690
C             X1 DENOTES THE REGION TOWARD THE END OF NODE 1 IN X-DIR.  THE01700
C     BELY1 : SAME AS ABOVE, AT Y1                                       THE01710
C     BELZ1 : SAME AS ABOVE, AT Z1                                       THE01720
C                                                                        THE01730
      READ(5,102) BELXN,BELYN,BELZN                                      THE01740
C     BELXN : THICKNESS OF ELECTROLYTE IN BOUNDARY REGION AT XN (M);    THE01750
C             XN DENOTES THE REGION TOWARD THE END OF NODE N IN X-DIR.  THE01760
C     BELYN : SAME AS ABOVE, AT YN                                       THE01770
C     BELZN : SAME AS ABOVE, AT ZN                                       THE01780
C                                                                        THE01790
      READ(5,101) STVS,CURTD,CURTC,RQL                                   THE01800
C     STVS  : MOLAR VOLUME CHANGE AS SOLID REACTANTS CONVERT TO PRODUCTSTHE01810
C             DUE TO ELECTROCHEMICAL REACTION (M**3/MOLE)                THE01820
C     CURTD : TOTAL CURRENT DURING DISCHARGE (AMPERE)                    THE01830
C     CURTC : TOTAL CURRENT DURING CHARGE (AMPERE)                       THE01840
C     RQL   : RATED AH CAPACITY (AMPERE-HOUR)                            THE01850
C                                                                        THE01860
      READ(5,101) Q,AQ1,AQ2,AQ3                                          THE01870
C     Q     : INITIAL STATE-OF-CHARGE (1.--0)                            THE01880
C     AQ1   : 1ST COEFFICIENT FOR CALCULATING HEAT OF DISCG. REACTION    THE01890
C             BY THE EQUATION  DHR=AQ1+AQ2*Q+AQ3*Q**2                    THE01900
C     AQ2   : 2ND COEFFICIENT IN ABOVE EQUATION                          THE01910
C     AQ3   : 3RD COEFFICIENT IN ABOVE EQUATION                          THE01920
C                                                                        THE01930
C    V-T CURVE FOR DISCHARGE OR CHARGE                                   THE01940
C                                                                        THE01950
      READ(5,106) COE1,COE2,COE3,COE4,COE5,SQL                           THE01960
C     COE1-COE5: COEFFICIENTS IN SHEPHERD'S EQUATION FOR DISCHARGE;      THE01970
C                SHEPHERD'S EQUATION USED TO PROVIDE CELL VOLTAGE BY     THE01980
C                V=COE1-COE2*CUR*(1/Q)-COE3*CUR+COE4*EXP(-1*COE5*(1-Q)) THE01990
C                WHERE Q IS STATE-OF-CHARGE AT ANY TIME BASED ON SQL.    THE02000
C     SQL   : AMPERE-HOUR CAPACITY USED AS A BASE FOR STATE-OF-CHARGE    THE02010
C             CALCULATION IN SHEPHERD'S EQUATION                         THE02020
C                                                                        THE02030
      READ(5,106) COE6,COE7,COE8,COE9,COE10,SQLC                         THE02040
C     COE6-COE10: COEFFICIENTS IN SHEPHERD'S EQUATION FOR CHARGE         THE02050
C     SQLC  : AH CAPACITY BASE USED IN SHEPHERD'S EQUATION FOR CHARGE    THE02060
C                                                                        THE02070
      READ(5,108) POTCUT,EPS,XKRIT,NSIG,ITMAX0                           THE02080
C     POTCUT: CUT-OFF VOLTAGE FOR DISCHARGE (V/CELL)                     THE02090
C     EPS   : A SMALL NUMBER AS 1ST CONVERGENCE CRITERION FOR ZFLASE;    THE02100
C             ZFALSE IS A IMSL ROUTINE USED TO CALCULATE CUT-OFF TIME    THE02110
C             FOR DISCHARGE BY SOLVING SHEPHERD'S EQN. AT CUT-OFF VOLT.  THE02120
C             ZFALSE FINDS SOLUTION BY "REGULA FALSI" ITERATION.         THE02130
C     XKRIT : A NUMBER (.8-1.2) USED TO PROVIDE INITIAL GUESS FOR ZFALSETHE02140
C     NSIG  : 2ND CONVERGENCE CRITERION FOR ZFALSE; NO. SIGNIFI. DIGITS.THE02150
C     ITMAX0: MAXIMUM NO. OF ITERATIONS ALLOWED IN ZFALSE                THE02160
C                                                                        THE02170
      READ(5,103) L,M,N,IIL,ISTOL,NCELL,NPLAT,ITL                        THE02180
C     L     : NO. OF NODES IN X DIRECTION, FOR FINITE DIFFERENCE APPROX.THE02190
C     M     : NO. OF NODES IN Y DIRECTION                                THE02200
C     N     : NO. OF NODES IN Z DIRECTION                                THE02210
C     IIL   : NO. OF CELLS OR MODULES CONSIDERED IN MODELING             THE02220
C     ISTOL : TOTAL NO. OF SURFACES                                      THE02230
C     NCELL : NO. OF CELLS PER MODULE                                    THE02240
C     NPLAT : NO. OF POSITIVE+NEGATIVE PLATES PER CELL                   THE02250
C     ITL   : MAXIMUM NO. OF ITERATIONS ALLOWED IN TEMPERATURE ITERATIONTHE02260
C                                                                        THE02270
```

```
C     EXTERNAL CONDITIONS                                                THE02280
C                                                                        THE02290
      READ(5,101) VAIR,GAP,TSPECL,XNPLOT                                 THE02300
C     VAIR  : AVERAGE LINEAR VELOCITY OF COOLING AIR STREAM (M/SEC)      THE02310
C     GAP   : SIZE OF AIR GAP (DISTANCE) BETWEEM CELLS OR MODULES (M);   THE02320
C             GAP BECOMES INACTIVE INPUT IF NO AIR SPACE EXISTS          THE02330
C             BETWEEN CELLS OR MODULES                                   THE02340
C     TSPECL: SPECIAL TEMPERATURE (K) AT WHICH CERTAIN CELL SURFACES     THE02350
C             ARE TO MAINTAINED AT; NOT USED IN MOST CASES               THE02360
C     XNPLOT: NO. OF 3-D PLOT FOR TEMPERATURE DISTRIBUTION DESIRED       THE02370
C                                                                        THE02380
      READ(5,107) IDH,COEHP                                              THE02390
C     IDH   : AN INDICATER FOR SELECTING WAYS TO CALCULTE HEAT TRANSFER THE02400
C             COEFFICIENTS BETWEEN AIR STREAM AND CELL SURFACES;         THE02410
C             IDH=1; PREASSIGNED HEAT TRANSFER COEFF.                    THE02420
C             IDH=2; SIMPLE CORRELATION USED FOR INTERNAL FLOW           THE02430
C             IDH=OTHER; COEFF. CALCULATED BASED ON LOCAL REYNOLDS NO.   THE02440
C     COEHP : VALUES OF PREASSIGNED HEAT TRANSFER COEFFICIENTS;          THE02450
C             COEHP(I) HAS DIMENSION OF 6, ONE COEFF. TO EACH SURFACE    THE02460
C                                                                        THE02470
      READ(5,101) THERKA,THERDA,VISCOK,EMIT                              THE02480
C     THERKA: THERMAL CONDUCTIVUTY OF AIR (WATTS/M/K)                    THE02490
C     THERDA: THERMAL DIFFUSIVITY OF AIR (CONDUC/DENSITY/CP)(M**2/SEC)   THE02500
C     VISCOK: KINEMATIC VISCOSITY OF AIR (M**2/SEC)                      THE02510
C     EMIT  : EMISSIVITY OF BATTERY SURFACES                             THE02520
C                                                                        THE02530
      READ(5,101) BETA,THERKP,WP,DENWP                                   THE02540
C     BETA  : COEFFICIENT OF EXPANSION FOR AIR (1/K)                     THE02550
C     THERKP: THERMAL CONDUCTIVITY OF PLASTIC CELL CASE (WATTS/M/K)      THE02560
C     WP    : THICKNESS OF PLASTIC CELL CASE (M)                         THE02570
C     DENWP : DENSITY OF PLASTIC USED FOR CELL CASE (KG/M**3)            THE02580
C                                                                        THE02590
      READ(5,109) TERMR,TERMK                                            THE02600
C     TERMR : RADIUS OF TERMINAL (M)                                     THE02610
C     TERMK : THERMAL CONDUCTIVITY OF TERMAL (WATTS/M/K)                 THE02620
C                                                                        THE02630
      READ(5,104) IPLOT,IP,IWRT                                          THE02640
C     IPLOT : INDICATOR FOR PLOTTING OPTIONS                             THE02650
C             IPLOT=0; NO PLOT WILL BE GENERATED                         THE02660
C             IPLOT=OTHER; XNPLOT NO. OF PLOTS WILL BE GENERATED         THE02670
C     IP    : INDICATCR FOR SELECTING CROSECTION FOR 3-D PLOT            THE02680
C             IP=1; PLOT T-DISTRIBUTION FOR X-CROSECTION AT X=XL/2       THE02690
C             IP=2; PLOT FOR Y-CROSECTION AT Y=YL/2                      THE02700
C             IP=3; PLOT FOR Z-CROSECTION AT Z=ZL/2                      THE02710
C     IWRT  : IWRT=0; NO DETAIL OUTPUT OF 3-D TEMPERATURE DIS.           THE02720
C             IWRT=OTHER; XNWRT NO. OF DETAIL T-DIS. WILL BE PRINTED.    THE02730
```

A sample calculation using the battery thermal model and input data as defined above is given in the Appendix. The calculation is made for a 150-Ah nickel/iron single cell during a 75-A constant-current discharge.

VI. CONCLUSION

A generic three-dimensional thermal model was developed for analyzing the thermal behavior of electric-vehicle batteries. The model calculates temperature distribution and excursion of a battery during discharge, charge, and open circuit. The model predictions agreed well with the temperature distributions measured in nickel/iron batteries.

Application of the thermal model to various nickel/iron batteries indicated that excessive temperature rise will occur in a closely packed 330-Ah module of five cells. Forced air convection is not effective for cooling the module. To facilitate the use of the model by EV designers and battery developers, the flow diagram for the model computer code and the input/output specifications are described. A sample calculation is also given to illustrate the procedures of using the model for battery thermal analysis.

ACKNOWLEDGMENT

This work was supported by the Department of Energy, Division of Electric and Hybrid Vehicles.

REFERENCES

1. S. M. Caulder and A. C. Simon, J. Electrochem. Soc. 121, 1546 (1974).

2. D. Berndt, The Effect of Temperature and Current Density on the Utilization of Lead and Lead Oxide Electrodes, Proc. of 6th Int. Power Sources Symp., Vol. 2, Brighton, U.K., p. 17 (1970)

3. N. J. Maskalick, J. Electrochem. Soc. 122(1), 19 (1975).

4. M. C. H. McKubre and D. D. MacDonald, J. Energy 5(6), 368 (1981).

5. E. C. Gay, J. D. Arntzen, D. R. Fredrickson, C. C. Christianson, F. Hornstra, and N. P. Yao, Impact of Temperature on Cycle Life of Globe ISOA EV-3000 Lead-Acid Batteries, Ext. Abs., Electrochem. Soc. Meeting, New Orleans, Vol. 84-2, pp. 55-56 (1984).

6. D. Gidaspow and B. S. Baker, AIChE J. 11(5), 825-831 (1965).

7. B. S. Baker, D. Gidaspow, and D. Wasan, Advances in Electrochemistry and Electrochemical Engineering, Vol. 8, John Wiley and Sons, New York, p. 63 (1971).

8. K. W. Choi and N. P. Yao, J. Electrochem. Soc. 125, 1011 (1978).

9. K. W. Choi and N. P. Yao, J. Electrochem. Soc. 126, 1321 (1979).

10. C. C. Chen and H. F. Gibbard, Thermal Management of Battery Systems for Electric Vehicle and Utility Lead Leveling, Proc. of 14th Intersoc. Energy Conversion Conf., Vol. 1, Aug. 5-10, 1979, Boston, MA, p. 725 (1979).

11. H. F. Gibbard and C. C. Chen, Thermal Management of Batteries, Proc. of the 12th Int. Power Sources Symp., Vol. 8, Brighton, U.K., p. 263 (1981).

12. N. P. Yao, AIChE Symp. Series 77(204), 129 (1981).

13. J. Lee, K. W. Choi, C. C. Christianson, and N. P. Yao, Three-Dimensional Thermal Modeling of EV Batteries, Ext. Abst., Electrochem. Soc. Mtg., Vol. 82-2, Detroit, MI, p. 5 (1982).

14. K. W. Choi and N. P. Yao, An Engineering Analysis of Thermal Phenomena for Lead-Acid Batteries during Recharge Processes, Argonne National Laboratory Report ANL-77-24 (1977).

15. H. F. Gibbard, J. Electrochem. Soc., 125, 353 (1978).

16. D. Bernardi, E. Pawlikowski, and J. Newman, J. Electrochem. Soc. 132, 5 (1985).

17. Eagle-Picher Industries, Inc., Annual Report on Research, Development and Demonstration of Nickel/Iron Batteries for Electric Vehicle Propulsion, Report Nos. ANL/OEPM-78-13, -79-13, -80-16, -81-13, (1978-1982)

18. B. Carnaham, H. A. Luther, and J. O. Wilkes, Applied Numerical Methods, John Wiley and Sons, New York (1969).

19. Globe Battery Division, Johnson Controls, Inc., Annual Report for 1983 on Research, Development, and Demonstration of Lead-Acid Batteries for Electric Vehicle Propulsion, Argonne National Laboratory Report ANL/OEPM-84-2 (1984).

20. J. Lee, C. C. Christianson, and N. P. Yao, Soc. of Automotive Engineers, Technical Paper Series No. 840473, p. 1-7 (1984).

21. J. Lee, R. Biwer, W. DeLuca, C. C. Christianson, and N. P. Yao, Final Report on Thermal Characterization of GM Nickel/Iron Cells, in preparation.

APPENDIX

SAMPLE CALCULATION

A sample calculation using the ANL battery thermal model "THERMO" is given below. The calculation is made for a 150-Ah nickel/iron single cell during a 75-A constant-current discharge. All cell surfaces are exposed to cooling air at a temperature of 25°C. The cooling air velocity is 5 m/s coming down from the top surface of the cell. The set of input data (defined on pp. 23-25) is

```
     40.0           0.2450        0.0490        0.1830
     25.00      13000.00      19000.00
     25.00          3.0       18000.0
     12.00          1.45          9.00
      1.00          1.00          0.00
      0.00000       0.000         0.000      1250.0
      0.03135  285786.60        168.12         32.90
      4.45          0.120         0.180         0.00080
   3200.00        800.00       1463.00          0.60
      0.025         0.0           0.0
      0.0126        0.00262       0.0066
      0.0126        0.00262       0.0066
      0.00        -75.00         40.00        150.0
      1.0     -286330.0           0.0           0.0
 1.256900    0.00034558  0.00008486  0.191810   22.519000   180.
 1.327260   -0.00045079  0.00002344 -0.047801   15.675300   180.
      1.00          0.00001       1.01         8   50
  9    9    9    1    6    1   16   20
      5.00          0.005        25.0           2.0
  0  15.00     15.00     28.00      10.00     16.00      16.00
      0.027         0.000025      0.000017      2.80
      0.0037        0.173         0.0024     1100.00
      0.0075       78.0
  1    1    1
 00   00   00   00   00   00
  0    0    0    0    0    0
```

Thus, the first row above gives values for XNSTEP, RXL, RYL, and RZL; the second row gives values for TINI, TIMEDL, and TIMECA; and so on.

Parts of the results directly taken from computer printout and plots are as follows:

```
NO. OF MODULES IN THE BATTERY :     1

NO. OF CELLS PER MODULE :  1
NO. OF PLATES PER CELL  : 16

DIMENSIONS OF MODULE OR CELL:  XL=  0.24500  YL=  0.04900  ZL=  0.18300

WEIGHT OF MODULE =      4.45000
VOLUME OF MODULE =      0.00220
DENSITY OF MODULE=  2025.56767


DIMENSIONS OF BATTERY CORE  :  XL=  0.19000  YL=  0.03896  ZL=  0.16500

APPROXIMATION MESH NO.  :     9    9    9
NUMBER OF TIME-STEPS    :    40.0

ARRANGEMENT IDENTIFICATION IIN(II,I) & IDIVID(II,I):
     0    0    0    0    0    0
     0    0    0    0    0    0


INITIAL TEMPERATURE :    25.0000
AMBIENT TEMPERATURE :    25.0000
AIR VELOCITY (M/S)  :     5.0000
ELECTROLYTE FLOW UX : 0.0
                 UY : 0.0
                 UZ : 0.0
GAP BETWEEN MODULES :     0.0050
INITIAL STA-O-CHARGE:     1.0000
RATED CAPACITY (AH) :     150.00

TIME STEP SIZE=       190.0000
MAX. TIME LIM.=     18000.0000
TIME-DISCHARGE=     13000.0000
TIME-CHARGE   =     19000.0000

CUT-OFF VOLT. =         1.0000
TIME TERMINATE=      7746.1693
AVG. CELL VOLT=         1.1945
AH DISCHARGED =       161.3785
WH DISCHARGED =       192.7588
SPECIFIC ENERGY (WH/KG)=         43.3166
SPECIFIC POWER  (W/KG) =         20.1312
VOL. ENERGY (WH/LITER) =         87.7407
VOL. POWER  (W/LITER)  =         40.7771

CHARGE CURRENT (AMP)           =   40.0000
CHARGE CURRENT EFFICIENCY      =    1.0000
DISCHARGE CURRENT (AMP)        =  -75.0000
DISCHARGE CURRENT EFFICIENCY=       1.0000
GAS EVOLUTION COEFFICIENT      =    0.0

SPECIFIC HEAT OF ELECTROLYTE  =     0.32000D+04
AVERAGE SPECIFIC HEAT OF SOLID=     0.80000D+03
SPECIFIC HEAT OF CELL CASE    =     0.14630D+04


VOLUME ELECTROLYTE PER CELL   =     0.80000D-03
VOL. ELTY. IN BOUNDARY        =     0.47361D-03
DENSITY OF ELECTROLYTE        =     0.12500D+04
THICKNESS OF CELL CASE        =     0.24000D-02
DENSITY OF CASE MATERIAL      =     0.11000D+04
THERMAL CONDUCTIVITY OF CASE  =     0.17300D+00


WEIGHT OF TERMINAL =     0.12000D+00
       OF COVER    =     0.18000D+00
       OF CELL CASE=     0.33549D+00
       OF BND ELTY.=     0.59202D+00
       OF COR ELTY.=     0.40793D+00
       OF COR SOLID=     0.28145D+01
WEIGHT OF CORE     =     0.32225D+01


EFFECTIVE THERMAL MASS OF CORE=     0.29124D+07
UNIT-ELECTROD GROSS THICKNESS =     0.25973D-02
SUPERFICIAL ELECTRODE AREA    =     0.31350D-01
```

```
THERMAL CONDUCTIVITY;     KX=   12.0000   KY=    1.4500   KZ=    8.0000

BOUNDARY AIR SPACE      :  XLAIR=      0.0250    YLAIR=      0.0        ZLAIR=      0.0
BOUNDARY MASS THICKNESS:  BTHX1=      0.0150    BTHXN=      0.0150
                          BTHY1=      0.0050    BTHYN=      0.0050
                          BTHZ1=      0.0090    BTHZN=      0.0090
BOUNDARY MASS DENSITY   :  BDEX1=   1192.0230    BDEXN=   1210.6760
                          BDEY1=   1177.2915    BDEYN=   1177.2915
                          BDEZ1=   1206.1914    BDEZN=   1206.1914
BOUNDARY SPECIFIC HEAT :  BCPX1=   2580.4559    BCPXN=   2786.2564
                          BCPY1=   2413.3123    BCPYN=   2413.3123
                          BCPZ1=   2737.3582    BCPZN=   2737.3582

EXPANSION COEFFICIENT BETA  =    0.37000D-02
AIR THERMAL CONDUCTIVITY    =    0.27000D-01
AIR VISCOSITY               =    0.17000D-04
RADIATIVE EMISIVITY         =    0.80000D+00

HEAT OF REACTION =-286330.00 +      0.0  * Q +      0.0  * Q * Q
DELT CP OF MAIN REACTION:      0.16812D+03
HEAT OF GASSING REACTION:      0.28579D+06
DELT CP OF GASSING RXN  :      0.32900D+02
DISCHARGE CELL VOLTAGE= COE1-COE2*I/(1-I*T/SQL)-COE3*I+COE4*DEXP(-COE5*(I*T/SQL))
      SQL  = 0.64800000D+06
      COE1= 0.12569000D+01
      COE2= 0.34558000D-03
      COE3= 0.84860000D-04
      COE4= 0.19181000D+00
      COE5= 0.22519000D+02

CHARGE CELL VOLTAGE= COE6-COE7*I/(1-I*T/SQLC)-COE8*I+COE9*DEXP(-COE10*(I*T/SQLC))
      SQLC= 0.18000000D+03
      COE6= 0.13272600D+01
      COE7=-0.45079000D-03
      COE8= 0.23440000D-04
      COE9=-0.47801000D-01
      COE10=0.15675300D+02

**** SPACE AROUND EACH MODULE: ****

0.500000000D+00  0.500000000D+00  0.500000000D+00  0.500000000D+00
0.500000000D+00  0.500000000D+00  0.500000000D+00  0.500000000D+00
0.500000000D+00  0.500000000D+00  0.500000000D+00  0.500000000D+00
0.500000000D+00  0.500000000D+00  0.500000000D+00  0.500000000D+00
0.500000000D+00  0.500000000D+00  0.500000000D+00  0.500000000D+00
0.500000000D+00  0.500000000D+00  0.500000000D+00  0.500000000D+00
0.500000000D+00  0.500000000D+00  0.500000000D+00  0.500000000D+00
0.500000000D+00  0.500000000D+00  0.500000000D+00  0.500000000D+00
0.500000000D+00  0.500000000D+00  0.500000000D+00  0.500000000D+00
0.500000000D+00  0.500000000D+00  0.500000000D+00  0.500000000D+00
0.500000000D+00  0.500000000D+00  0.500000000D+00  0.500000000D+00
0.500000000D+00  0.500000000D+00  0.500000000D+00  0.500000000D+00
0.500000000D+00  0.500000000D+00  0.500000000D+00  0.500000000D+00
0.500000000D+00  0.500000000D+00  0.500000000D+00  0.500000000D+00
0.500000000D+00  0.500000000D+00  0.500000000D+00  0.500000000D+00
0.500000000D+00  0.500000000D+00  0.500000000D+00  0.500000000D+00
0.500000000D+00  0.500000000D+00  0.500000000D+00  0.500000000D+00
0.500000000D+00  0.500000000D+00  0.500000000D+00  0.500000000D+00
0.500000000D+00  0.500000000D+00  0.500000000D+00  0.500000000D+00
0.500000000D+00  0.500000000D+00  0.500000000D+00  0.500000000D+00
0.500000000D+00  0.500000000D+00  0.500000000D+00  0.500000000D+00
0.500000000D+00  0.500000000D+00  0.500000000D+00  0.500000000D+00
0.500000000D+00  0.500000000D+00  0.500000000D+00  0.500000000D+00
0.500000000D+00  0.500000000D+00  0.500000000D+00  0.500000000D+00
```

```
********** TIME =     10.00   **********


  DIMENSIONLESS GROUPS:

     INTERNAL CONDUCTION:    COEFX=   0.8841285D+00    COEFY=   0.2540806D+01    COEFZ=   0.7815620D+00
     INTERNAL CONVECTION:    COEFUX=  0.0              COEFUY=  0.0              COEFUZ=  0.0
     HEAT GENERATION:        COEFG=  -0.6546336D+00    COEFH=   0.8132010D+00    COEFT=   0.1585674D+00
                             COECP=   0.0              COEF8=   0.2173544D+00    COEF9=   0.0
     BOUNDARY MASS:          TMSX1=   0.9430999D-01    TMSXN=   0.1034250D+00    TMSY1=   0.4947265D-01
                             TMSYN=   0.4947265D-01    TMSZ1=   0.7912201D-01    TMSZN=   0.7912201D-01

                             TMSYN=   0.4947265D-01    TMSZ1=   0.7912201D-01    TMSZN=   0.7912201D-01
     SURFACE RADIATION:      SELX =   0.1901286D-01    SELY =   0.3226458D-01    SELZ =   0.2476675D-01

     TAMB =   0.1000000D+01


*** HEAT TRANSFER COEFFICIENTS (WATTS/M/M/K): ***


                      ENTRY LENGTH=  0.0           0.0           0.24500D+00
     1     1     2  0.27037D+02  0.27037D+02  0.27037D+02  0.27037D+02
     1     1     4  0.14384D+02  0.14384D+02  0.14384D+02  0.14384D+02
     1     1     6  0.10977D+02  0.10977D+02  0.10977D+02  0.10977D+02
     1     1     8  0.92196D+01  0.92196D+01  0.92196D+01  0.92196D+01
                      ENTRY LENGTH=  0.0           0.0           0.24500D+00
     1     2     2  0.27037D+02  0.27037D+02  0.27037D+02  0.27037D+02
     1     2     4  0.14384D+02  0.14384D+02  0.14384D+02  0.14384D+02
     1     2     6  0.10977D+02  0.10977D+02  0.10977D+02  0.10977D+02
     1     2     8  0.92196D+01  0.92196D+01  0.92196D+01  0.92196D+01
                      ENTRY LENGTH=  0.0           0.0           0.24500D+00
     1     3     2  0.28004D+02  0.28004D+02  0.28004D+02  0.28004D+02
     1     3     4  0.28004D+02  0.28004D+02  0.28004D+02  0.28004D+02
     1     3     6  0.28004D+02  0.28004D+02  0.28004D+02  0.28004D+02
     1     3     8  0.28004D+02  0.28004D+02  0.28004D+02  0.28004D+02
                      ENTRY LENGTH=  0.0           0.0           0.24500D+00
     1     4     2  0.60490D+01  0.60490D+01  0.60490D+01  0.60490D+01
     1     4     4  0.60490D+01  0.60490D+01  0.60490D+01  0.60490D+01
     1     4     6  0.60490D+01  0.60490D+01  0.60490D+01  0.60490D+01
     1     4     8  0.60490D+01  0.60490D+01  0.60490D+01  0.60490D+01
                      ENTRY LENGTH=  0.0           0.0           0.24500D+00
     1     5     2  0.27037D+02  0.27037D+02  0.27037D+02  0.27037D+02
     1     5     4  0.14384D+02  0.14384D+02  0.14384D+02  0.14384D+02
     1     5     6  0.10977D+02  0.10977D+02  0.10977D+02  0.10977D+02
     1     5     8  0.92196D+01  0.92196D+01  0.92196D+01  0.92196D+01
                      ENTRY LENGTH=  0.0           0.0           0.24500D+00
     1     6     2  0.27037D+02  0.27037D+02  0.27037D+02  0.27037D+02
     1     6     4  0.14384D+02  0.14384D+02  0.14384D+02  0.14384D+02
     1     6     6  0.10977D+02  0.10977D+02  0.10977D+02  0.10977D+02
     1     6     8  0.92196D+01  0.92196D+01  0.92196D+01  0.92196D+01

    HAVG(II,I):      0.14557D+02  0.14557D+02  0.28004D+02  0.60490D+01  0.14557D+02  0.14557D+02
    BIOT(II,I):      0.30024D+00  0.30024D+00  0.44339D+00  0.95776D-01  0.39114D+00  0.39114D+00
    CBAVG(II,I):     0.74155D+00  0.74155D+00  0.43756D+00  0.82580D+00  0.79523D+00  0.79523D+00

  STATE-OF-CHARGE =    0.99884
  TOTAL CURRENT   = -75.00000
  CURRENT DENSITY =-159.48963
  BATTERY VOLTAGE =    1.41146
  CELL VOLTAGE    =    1.41146

     TIME =  0.129D-02   KPASS=  1
     TIME =  0.129D-02   KPASS=  2

TA(II,I) =     298.0073     298.0073     298.0043     298.0073     298.0067     298.0067     298.0126     298.0130
```

```
********** TIME =   7660.00   **********

     HAVG(II,I):      0.14557D+02  0.14557D+02  0.28004D+02  0.60490D+01  0.14557D+02  0.14557D+02
     BIOT(II,I):      0.30024D+00  0.30024D+00  0.44339D+00  0.95776D-01  0.39114D+00  0.39114D+00
     CBAVG(II,I):     0.74155D+00  0.74155D+00  0.43844D+00  0.82580D+00  0.79523D+00  0.79523D+00

  STATE-OF-CHARGE =    0.11343
  TOTAL CURRENT    = -75.00000
  CURRENT DENSITY =-159.48963
  BATTERY VOLTAGE =    1.02203
  CELL VOLTAGE    =    1.02203

     TIME =  0.989D+00   KPASS= 1
     TIME =  0.989D+00   KPASS= 2
     TIME =  0.989D+00   KPASS= 3
     TIME =  0.989D+00   KPASS= 4
     TIME =  0.989D+00   KPASS= 5

TA(II,I) =    309.1412    309.1412    304.2919    310.9986    309.7572    309.7572    314.1381    314.3230

********** TIME =   7746.17   **********

     HAVG(II,I):      0.14557D+02  0.14557D+02  0.28004D+02  0.60490D+01  0.14557D+02  0.14557D+02
     BIOT(II,I):      0.30024D+00  0.30024D+00  0.44339D+00  0.95776D-01  0.39114D+00  0.39114D+00
     CBAVG(II,I):     0.74155D+00  0.74155D+00  0.43845D+00  0.82580D+00  0.79523D+00  0.79523D+00

  STATE-OF-CHARGE =    0.10345
  TOTAL CURRENT    = -75.00000
  CURRENT DENSITY =-159.48963
  BATTERY VOLTAGE =    1.00000
  CELL VOLTAGE    =    1.00000

     TIME =  0.100D+01   KPASS= 1
     TIME =  0.100D+01   KPASS= 2
     TIME =  0.100D+01   KPASS= 3

HEAT GENERATION RATE:
  QDOT NON-DIMEN.:  0.25754D+00
  WATTS/M3   (II):  0.28855D+05
  WATTS      (II):  0.35243D+02
  WH-THIS STEP   :  0.84358D+00
  WH-GENERATED   :0.4618835D+02

HEAT DISSIPATION BY CONVECTION:
  WATTS/M2(I) : 0.1561962D+03 0.1561962D+03 0.1790621D+03 0.7985512D+02 0.1657473D+03 0.1657473D+03
  WATTS   (I) : 0.1156227D+01 0.1156227D+01 0.1151083D+01 0.5133406D+00 0.5196179D+01 0.5196179D+01
  WH-THIS STEP: 0.2767534D-01 0.2767534D-01 0.2755222D-01 0.1228728D-01 0.1243753D+00 0.1243753D+00
  WH-UP TO T  : 0.1373396D+01 0.1373396D+01 0.1374742D+01 0.6037979D+00 0.6182987D+01 0.6182987D+01

  WH-UP TO T  : 0.1373396D+01 0.1373396D+01 0.1374742D+01 0.6037979D+00 0.6182987D+01 0.6182987D+01
  SUM OF SURFACES: THIS STEP= 0.3439407D+00 (WH)   40.7716 %
                   UP-TO-T=   0.1709131D+02 (WH)   37.0035 %

HEAT DISSIPATION BY RADIATION:
  WATTS/M2(I) : 0.5761033D+02 0.5761033D+02 0.3172006D+02 0.6775760D+02 0.6097771D+02 0.6097771D+02
  WATTS   (I) : 0.4264547D+00 0.4264547D+00 0.2039092D+00 0.4355730D+00 0.1911651D+01 0.1911651D+01
  WH-THIS STEP: 0.1020758D-01 0.1020758D-01 0.4880753D-02 0.1042584D-01 0.4575711D-01 0.4575711D-01
  WH-UP TO T  : 0.4967523D+00 0.4967523D+00 0.2410969D+00 0.5019022D+00 0.2228787D+01 0.2228787D+01
  SUM OF SURFACES: THIS STEP= 0.1272360D+00 (WH)   15.0829 %
                   UP-TO-T=   0.6194077D+01 (WH)   13.4105 %

TOTAL HEAT DISSIPATION: THIS STEP= 0.4711767D+00 (WH)   55.8545 %
                        UP-TO-T=   0.2328538D+02 (WH)   50.4140 %
```

```
LOCAL TEMPERATURE DISTRIBUTIONS (K):


II =      1
 TS=
 J =   8                   0.3061D+02    0.3109D+02    0.3109D+02    0.3061D+02
 J =   6                   0.3133D+02    0.3188D+02    0.3188D+02    0.3133D+02
 J =   4                   0.3133D+02    0.3188D+02    0.3188D+02    0.3133D+02
 J =   2                   0.3061D+02    0.3109D+02    0.3109D+02    0.3061D+02

 I =      2
                           0.3357D+02    0.3430D+02    0.3430D+02    0.3357D+02
 J =   8     0.3265D+02    0.3780D+02    0.3889D+02    0.3889D+02    0.3780D+02    0.3265D+02
 J =   6     0.3364D+02    0.3945D+02    0.4069D+02    0.4069D+02    0.3945D+02    0.3364D+02
 J =   4     0.3364D+02    0.3945D+02    0.4069D+02    0.4069D+02    0.3945D+02    0.3364D+02
 J =   2     0.3265D+02    0.3780D+02    0.3889D+02    0.3889D+02    0.3780D+02    0.3265D+02
                           0.3357D+02    0.3430D+02    0.3430D+02    0.3357D+02

 I =      4
                           0.3635D+02    0.3722D+02    0.3722D+02    0.3635D+02
 J =   8     0.3556D+02    0.3933D+02    0.4042D+02    0.4042D+02    0.3933D+02    0.3556D+02
 J =   6     0.3665D+02    0.4082D+02    0.4203D+02    0.4203D+02    0.4082D+02    0.3665D+02
 J =   4     0.3665D+02    0.4082D+02    0.4203D+02    0.4203D+02    0.4082D+02    0.3665D+02
 J =   2     0.3556D+02    0.3933D+02    0.4042D+02    0.4042D+02    0.3933D+02    0.3556D+02
                           0.3635D+02    0.3722D+02    0.3722D+02    0.3635D+02

 I =      6
                           0.3751D+02    0.3838D+02    0.3838D+02    0.3751D+02
 J =   8     0.3680D+02    0.4002D+02    0.4106D+02    0.4106D+02    0.4002D+02    0.3680D+02
 J =   6     0.3788D+02    0.4139D+02    0.4255D+02    0.4255D+02    0.4139D+02    0.3788D+02
 J =   4     0.3788D+02    0.4139D+02    0.4255D+02    0.4255D+02    0.4139D+02    0.3788D+02
 J =   2     0.3680D+02    0.4002D+02    0.4106D+02    0.4106D+02    0.4002D+02    0.3680D+02
                           0.3751D+02    0.3838D+02    0.3838D+02    0.3751D+02

 I =      8
                           0.3747D+02    0.3829D+02    0.3829D+02    0.3747D+02
 J =   8     0.3685D+02    0.3957D+02    0.4053D+02    0.4053D+02    0.3957D+02    0.3685D+02
 J =   6     0.3786D+02    0.4081D+02    0.4186D+02    0.4186D+02    0.4081D+02    0.3786D+02

 J =   6     0.3786D+02    0.4081D+02    0.4186D+02    0.4186D+02    0.4081D+02    0.3786D+02
 J =   4     0.3786D+02    0.4081D+02    0.4186D+02    0.4186D+02    0.4081D+02    0.3786D+02
 J =   2     0.3685D+02    0.3957D+02    0.4053D+02    0.4053D+02    0.3957D+02    0.3685D+02
                           0.3747D+02    0.3829D+02    0.3829D+02    0.3747D+02
 TS=
 J =   8                   0.3703D+02    0.3783D+02    0.3783D+02    0.3703D+02
 J =   6                   0.3806D+02    0.3892D+02    0.3892D+02    0.3806D+02
 J =   4                   0.3806D+02    0.3892D+02    0.3892D+02    0.3806D+02
 J =   2                   0.3703D+02    0.3783D+02    0.3783D+02    0.3703D+02


LOCAL HEAT SOURCE DISTRIBUTIONS (JOUL/SEC/M**3):


II =      1

 I =      2
 J =   8    0.2902D+05    0.2896D+05    0.2896D+05    0.2902D+05
 J =   6    0.2893D+05    0.2887D+05    0.2887D+05    0.2893D+05
 J =   4    0.2893D+05    0.2887D+05    0.2887D+05    0.2893D+05
 J =   2    0.2902D+05    0.2896D+05    0.2896D+05    0.2902D+05

 I =      4
 J =   8    0.2894D+05    0.2888D+05    0.2888D+05    0.2894D+05
 J =   6    0.2886D+05    0.2880D+05    0.2880D+05    0.2886D+05
 J =   4    0.2886D+05    0.2880D+05    0.2880D+05    0.2886D+05
 J =   2    0.2894D+05    0.2888D+05    0.2888D+05    0.2894D+05
```

I	=	6				
J	=	8	0.2830D+05	0.2885D+05	0.2885D+05	0.2890D+05
J	=	6	0.2883D+05	0.2277D+05	0.2877D+05	0.2883D+05
J	=	4	0.2383D+05	0.2877D+05	0.2877D+05	0.2833D+05
J	=	2	0.2830D+05	0.2885D+05	0.2885D+05	0.2890D+05
I	=	8				
J	=	8	0.2893D+05	0.2888D+05	0.2888D+05	0.2893D+05
J	=	6	0.2886D+05	0.2880D+05	0.2880D+05	0.2886D+05
J	=	4	0.2886D+05	0.2880D+05	0.2880D+05	0.2886D+05
J	=	2	0.2893D+05	0.2888D+05	0.2888D+05	0.2893D+05

Temperature Distribution at x-Cross Section

Module: 1 Time=129.1 min

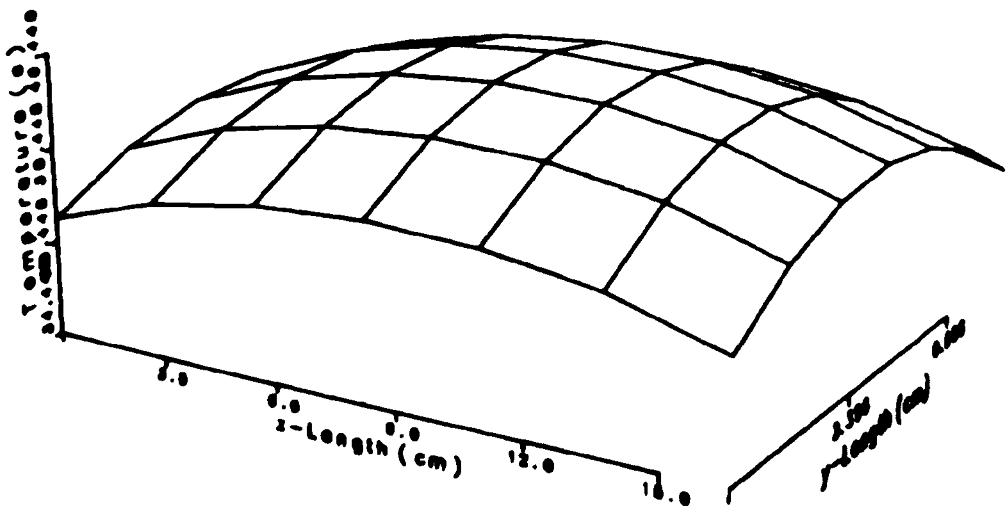

Temperature Profile Along x–Axis

Module: 1   Time Step= 43.0 min

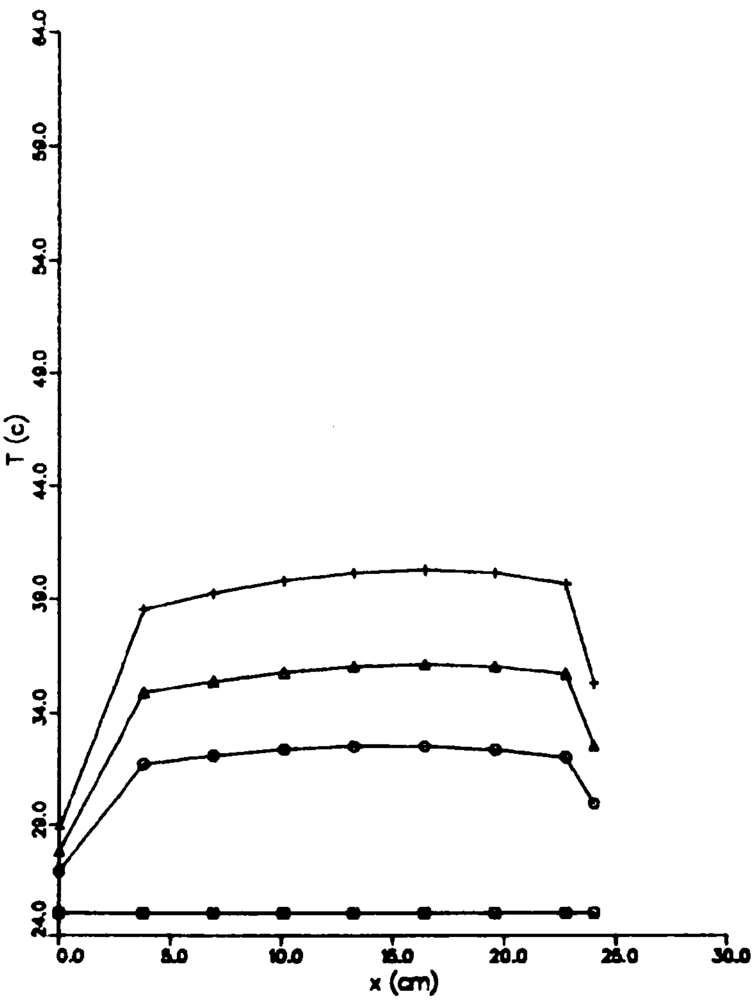

Temperature Profile Along y-Axis

Module: 1 Time Step= 43.0 min

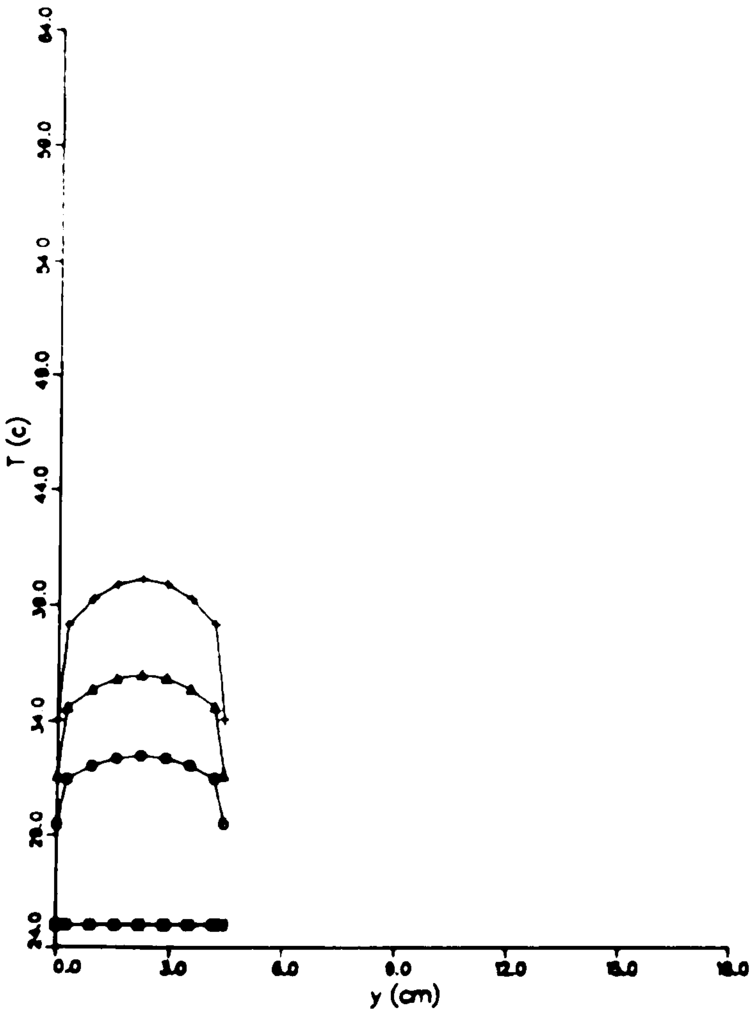

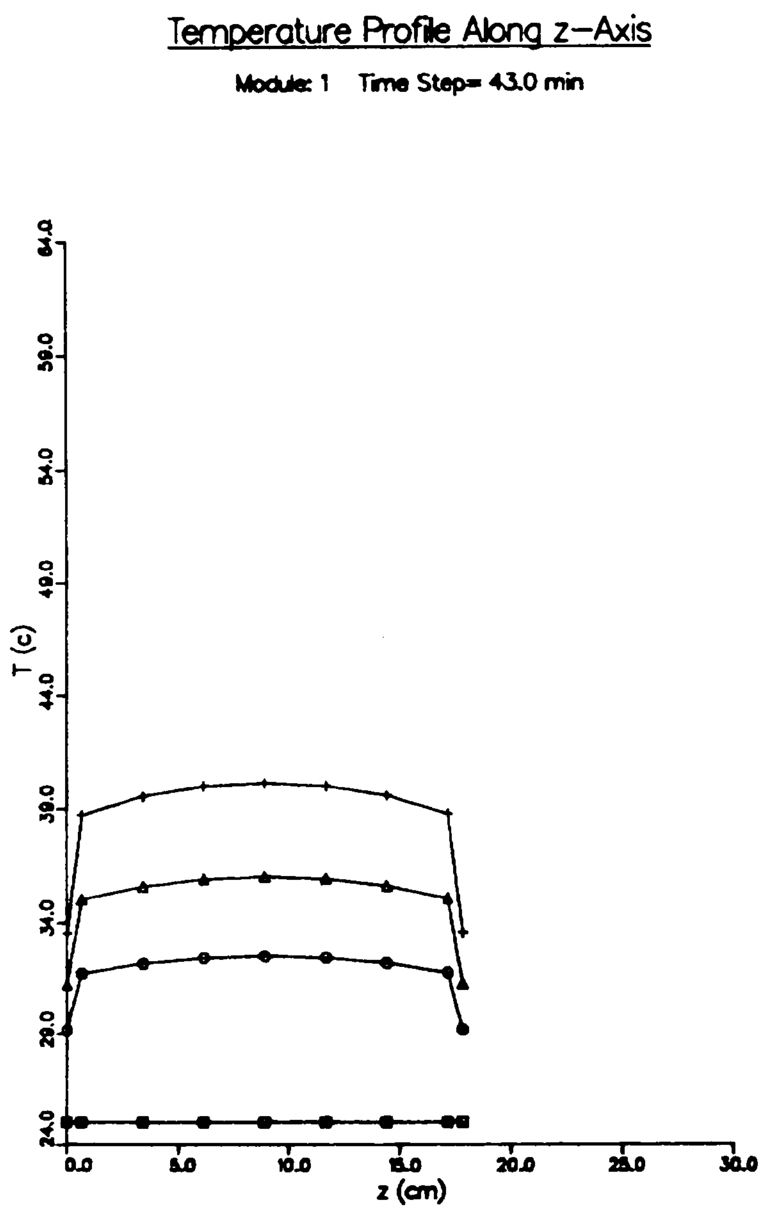
Temperature Profile Along z–Axis
Module: 1   Time Step= 43.0 min
T (c)
64.0
59.0
54.0
49.0
44.0
39.0
34.0
29.0
24.0
0.0
5.0
10.0
15.0
20.0
25.0
30.0
z (cm)

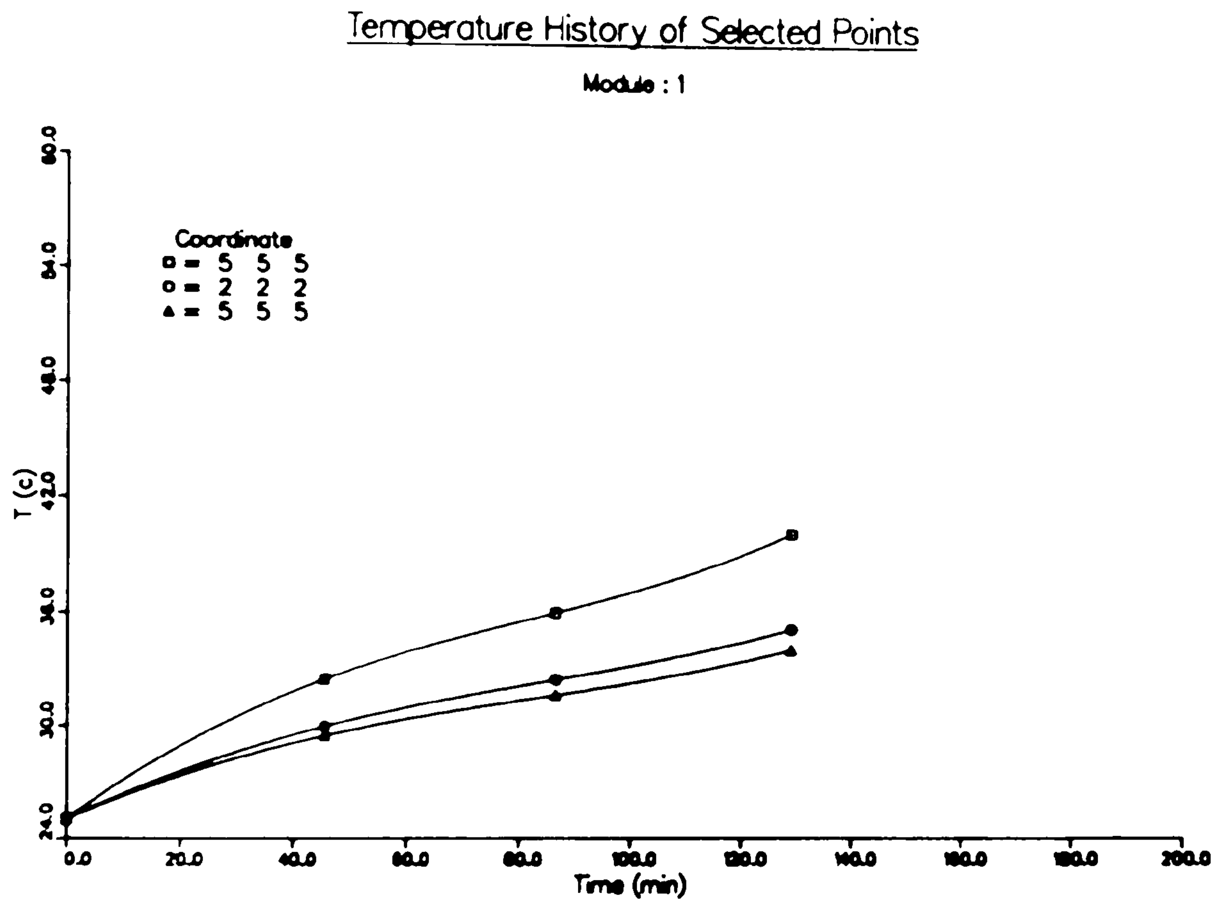
Temperature History of Selected Points
Module : 1
Coordinate
□ = 5 5 5
○ = 2 2 2
▲ = 5 5 5
T (c)
24.0
30.0
36.0
42.0
48.0
54.0
60.0
0.0
20.0
40.0
60.0
80.0
100.0
120.0
140.0
160.0
180.0
200.0
Time (min)

Distribution for ANL-85-53

Internal:

J. P. Ackerman
J. Battles
R. L. Breyne
A. A. Chilenskas
C. C. Christianson (5)
W. H. DeLuca
D. C. Fee
J. Harmon
F. Hornstra
J. Lee (10)
J. F. Miller
P. A. Nelson
R. D. Pierce
M. F. Roche
J. Smaga
J. L. Smith
M. J. Steindler
R. Varma
D. R. Vissers
ANL Patent Dept.
ANL Contract File
ANL Libraries
TIS Files (6)

External:

DOE-TIC, for distribution per UC-94ca (231)
Manager, Chicago Operations Office, DOE
R. Gariboldi, DOE-CH
H. Glenn, DOE-CH
Chemical Technology Division Review Committee Members:
S. Baron, Brookhaven National Lab.
W. L. Worrell, U. Pennsylvania
E. B. Yeager, Case Western Reserve U.
B. A. Askew, Los Altos, Calif.
K. F. Barber, Div. Electric and Hybrid Propulsion, USDOE
J. H. Barnett, Tennessee Valley Authority, Chattanooga
W. Bauer, KW Battery Co., Skokie, Ill.
R. J. Bellows, Exxon Research & Engineering Co., Linden, N. J.
D. N. Bennion, Brigham Young U., Provo
J. R. Birk, Electric Power Research Inst., Palo Alto
J. Broadhead, Bell Labs., Murray Hill, N. J.
E. P. Broglio, Eagle-Picher Industries, Inc., Joplin, Mo.
J. T. Brown, Westinghouse Electric Corp., Pittsburgh
P. J. Brown, Div. Electric and Hybrid Propulsion, USDOE
D. M. Bush, Sandia National Labs., Albuquerque
E. S. Buzzelli, Westinghouse Electric Corp., Pittsburgh
E. J. Cairns, Lawrence Berkeley Lab.
S. H. Caulder, Naval Research Lab.
K. W. Choi, Park Ridge, Ill.
R. P. Clark, Sandia National Labs., Albuquerque
J. F. Cooper, Lawrence Livermore National Lab.
R. Corbin, Delco Remy, Anderson, Ind.
A. N. Dey, Duracell Inc., Burlington, Mass.
W. J. Dippold, Div. Electric and Hybrid Propulsion, USDOE
J. B. Doe, GNB Batteries, Inc., Langhorne, Pa.
D. L. Douglas, Electric Power Research Inst., Palo Alto
E. Dowgiallo, Div. Electric and Hybrid Propulsion, USDOE
D. Edwards, Jet Propulsion Lab.
M. Eisenberg, Electrochimica Corp., Menlo Park
H. A. Fuggiti, Exide Corp., Yardley, Pa.
J. H. B. George, George Consulting International, Inc., Concord, Mass.
R. G. Gunther, General Motors Research Lab., Warren, Mich.
W. Hamilton, Santa Barbara, Calif.
J. Hardin, EG&G Idaho, Inc., Idaho Falls
R. A. Harlow, Ford Aerospace & Communications Corp., Newport Beach, Calif.

G. S. Hartman, Exide Corp., Yardley, Pa.
J. L. Hartman, General Motors Research Lab., Warren, Mich.
E. Hellmann, Energy Development Associates, Madison Heights, Mich.
J. S. Hodgman, General Electric Co., Gainesville
R. P. Hollandsworth, Lockheed Missile and Space Co., Palo Alto
R. Hudson, Eagle-Picher Industries, Inc., Joplin, Mo.
G. L. Hunt, EG&G Idaho, Inc.
R. S. Kirk, Div. Electric and Hybrid Propulsion, USDOE
A. R. Landgrebe, Div. Energy Utilization Research, USDOE
S. H. Langer, U. Wisconsin, Madison
V. R. Matricardi, Aerospace Corp., Washington
B. L. McKinney, Johnson Controls, Inc., Milwaukee
F. McLarnon, Lawrence Berkeley Lab.
R. H. Muller, Lawrence Berkeley Lab.
J. S. Newman, U. California, Berkeley
A. O. Nilsson, SAB NIFE Inc., Lincoln, R. I.
L. G. O'Connell, Electric Power Research Inst., Palo Alto
P. Patil, Div. Electric and Hybrid Propulsion, USDOE
J. E. Quinn, Div. Energy Utilization Research, USDOE
J. Rowlette, Jet Propulsion Lab.
J. R. Selman, Illinois Inst. Technology
E. T. Seo, The Gates Corp., Littleton, Colo.
J. Skorupski, Eaton Corp., Southfield, Mich.
P. Smith, Eaton Corp., Southfield, Mich.
W. Spindler, Electric Power Research Inst., Palo Alto
P. C. Symons, Electrochemical Engineering Consultants, Inc., Palo Alto
R. Thacker, General Motors Research Labs., Warren, Mich.
W. H. Tiedemann, Johnson Controls, Inc., Milwaukee
A. Uchiyama, Jet Propulsion Lab.
C. J. Venuto, C & D Power Systems Div., Allied Corp., Plymouth Meeting, Pa.
G. J. Walker, Div. Electric and Hybrid Propulsion, USDOE
C. E. Weinlein, Johnson Controls, Inc., Milwaukee
N. P. Yao, Clarendon Hills, Ill.
Chloride Technical Ltd., Library, Manchester, England